Electronic properties and stabilities of bulk and low-index surfaces of SnO in comparison with SnO$_2$: A first-principles density functional approach with an empirical correction of van der Waals interactions

Yuhua Duan[*]

National Energy Technology Laboratory, United States Department of Energy, Pittsburgh, Pennsylvania 15236, USA
and Parsons, P.O. Box 618, South Park, Pennsylvania 15129, USA

The electronic properties and stabilities of SnO and SnO$_2$ bulk materials and their low-index surfaces are investigated by density functional theory. An empirical method has been adopted in this study to account for the van der Waals interactions among the Sn-O layers in the bulk and low-index surfaces of SnO. Compared with SnO$_2$, the structural and electronic properties of SnO bulk and its low-index surfaces present some unique features due to the dual valency of Sn. In SnO, the *s* orbital of Sn has larger contributions than its *p* and *d* orbitals in the first valence band (VB) and the *p* orbital of Sn has a larger contribution than its *s* and *d* orbitals in its conduction band (CB). In SnO$_2$, the *p* and *d* orbitals of Sn play an important role to form the upper part of the VB and its *s* orbital dominates in forming the lower parts of the VB and the CB. In both oxides, the *s* orbital of O forms the second VB with lower energy and its *p* orbitals are involved in forming the first VB and the CB. The calculated bulk modulus and cohesive energy agree well with the experimental measurements. By constructing all possible symmetrical low-index surfaces of SnO and the (111) surface of SnO$_2$, our results reveal that the calculated surface energies of SnO stoichiometric surfaces are lower than that of the corresponding surfaces of SnO$_2$ due to different bonding between Sn and O in these two oxides. The calculated stabilities of the low-index stoichiometric surfaces of SnO are in the order $(001) > (101)/(011) \geq (010)/(100) > (110) > (111)$ while the order in the case of SnO$_2$ is $(110) > (010)/(100) > (101)/(011) > (001) > (111)$. The calculated relationships between surface free energies $[\gamma(p,T)]$ and oxygen chemical potentials $[\mu_O(p,T)]$ indicate that the nonstoichiometric O-terminated (110) and (111) surfaces of SnO could be more stable than their corresponding stoichiometric ones when the $\mu_O(p,T)$ reaches its higher O-rich bound, and one Sn-terminated nonstoichiometric (111) surface of SnO$_2$ could be more stable than its stoichiometric ones when the $\mu_O(p,T)$ falls into its lower O-poor region. During surface formation from the bulk, the stable surface usually has small atom displacements. For both SnO and SnO$_2$ the atoms on the (111) surface have larger relaxations than on their other low-index surfaces.

I. INTRODUCTION

As one of the wide-band-gap oxides, stannic oxide (SnO$_2$) is of interest for a variety of technical applications and widely used as solid state sensor materials, oxidation catalysts, and transparent conductors.[1–4] Due to its electronic structure and the possibility of two different oxidation states of Sn^{4+} and Sn^{2+}, SnO$_2$ are very sensitive to oxidizing and reducing many kinds of gases, such as O$_2$, CO, CO$_2$, NO$_x$, CH$_4$, H$_2$O, NH$_3$, BF$_3$, CH$_3$OH, C$_2$H$_4$, etc., and therefore can be used to detect these gases with good sensitivity. Since the SnO$_2$ melting point is very high (>1900 °C), it can be a good candidate for high-temperature sensor-related applications. Above 1500 °C, SnO$_2$ can be decomposed into SnO and O$_2$.[2] The main drawback to using SnO$_2$ as a sensor is its poor selectivity simply because it is sensitive to so many kinds of molecules. In order to overcome this drawback and let SnO$_2$ detect particular molecules, new technologies are used to make such kind of sensors for different purposes. There are mainly three kinds of technical methods to make SnO$_2$ related sensor materials: doping noble metal on SnO$_2$, growth of SnO$_2$ on other materials, and forming nanosize particles.[2,5] The bulk properties, low-index surfaces, and adsorptive properties of stannic oxide (SnO$_2$) have been extensively

investigated both by experimental and theoretical studies.[1–4,6–21] The surface composition indirectly influences the gas sensing mechanism. Different additives in SnO$_2$ can either increase the charge carrier concentration by donor atoms or decrease the surface conductivity responsible for the gas response signal. Therefore, doping different elements or growing other oxides on SnO$_2$ can improve the sensing selectivity of SnO$_2$. Many surface properties of SnO$_2$ are caused by the dual valency of Sn which facilitates a reversible transformation of surface composition (Sn$^{4+} \leftrightarrow$ Sn^{2+}).

Compared with extensive investigations on the bulk and surface properties of SnO$_2$, stannous oxide (SnO) has not attracted much interest among researchers. Part of the reason is that SnO undergoes rapid oxidation with incandescence to SnO$_2$ upon heating to around 300 °C as illustrated by Suito *et al.*[22] Moreover, several intermediate oxides between stannic and stannous oxides, such as Sn$_2$O$_3$, Sn$_3$O$_4$, and Sn$_5$O$_6$, have also been reported.[23] The heats of formation (ΔH) at 298 K for SnO and SnO$_2$ are -68 and -138 kcal/mol, respectively, which results in -70 kcal/mol for the reaction SnO(c)$+1/2$O$_2 \rightarrow$ SnO$_2$(c).[2,24] This indicates the stannic oxide is the thermodynamically most stable form among tin oxides. However, as mentioned above, the SnO$_2$ can be decomposed to SnO when the temperature goes higher than 1500 °C and on the surfaces of SnO$_2$ the reduced form of Sn

TABLE I. The optimized crystal structure [experimental crystal constants of SnO_2 (Ref. [2]): $a=b$ =4.7373 Å, c=3.1864 Å] and binding energy of SnO_2.

	PAW_PW91	PAW_d_PW91	PAW_PBE	PAW_d_PBE	US_PW91	US_d_PW91
a (Å)	4.821	4.823	4.826	4.828	4.820	4.821
c (Å)	3.236	3.241	3.237	3.242	3.228	3.234
Error (a,c) (%)	1.78, 1.56	1.80, 1.71	1.92, 1.76	1.91, 1.75	1.78, 1.35	1.78, 1.50
Binding energy (eV)	−18.937	−18.776	−18.770	−18.843	−18.931	−18.779

does exist. Therefore it is worth exploring thoroughly the structural and electronic properties of bulk and low-index surfaces of SnO and comparing them with SnO_2. X-ray photoelectron spectra analysis (XPS) showed that a shift of about 1 eV occurs in the binding energy from SnO_2 to SnO.[25] Using electron spectroscopy for chemical analysis to analyze the oxidation of tin, Lau and Wertheim[26] concluded that SnO and SnO_2 have the same chemical shift and to identify them one needs to compare their valence bands and O/Sn ratio. Using XPS, Themlin *et al.*[27] obtained a chemical shift of 0.7 ± 0.05 eV between formal Sn^{4+} and Sn^{2+} and a binding energy difference of 1.6 eV between SnO_2 and SnO. Resonant photoemission characterization of SnO showed that O $2p$, Sn $5s$, and $5p$ partial density of states are the main contributors to the valence band of this material.[28]

Several theoretical investigations focused on the stability properties of the SnO bulk materials. Meyer *et al.*[29] used *ab initio* pseudopotential calculations to study the equilibrium structure of SnO and found that different choices for Sn pseudopotential dramatically influenced the resulting equilibrium structure of SnO. By gradient corrected density functional theory, the SnO in the structures of litharge, idealized CsCl, rocksalt, and herzenbergite are being investigated.[30,31] Their results for SnO in the litharge structure are in good agreement with experimental findings which gives nonspherical electron distribution. The states responsible for asymmetric Sn electron distribution are due to the coupling of unfilled Sn($5p$) with antibonding combination arising from interaction of Sn($5s$) and O($2p$).[31] Recently, with *ab initio* full-potential linearized augmented planewave (FP-LAPW) method Errico[32] investigated the electronic structures of SnO and SnO_2 and calculated the electric-field gradient tensor at Sn sites. Unlike SnO_2, to our knowledge, up to now there has been no theoretical study on the low-index surfaces of SnO and their sensing properties with molecules. Moreover, the (111) surface of SnO_2 has rarely been studied in the literature. In this work, by *ab initio* density functional theory, we focus on exploring the electronic properties of bulk SnO and its low-index surfaces and comparing them with those of SnO_2.

This paper is organized as follows: in Sec. II we briefly describe the theoretical method we employed and show the differences when choosing different pseudopotentials and exchange-correlation functions. In Sec. III we first show our results for the bulk materials of SnO and SnO_2, then present the results for the low-index [(001), (100), (010), (110), (011), (101), and (111)] surfaces of SnO and compare them with the corresponding surfaces of SnO_2. We discuss the differences between these two oxides, and in Sec. IV summarize our conclusions.

II. THEORETICAL METHODS

The calculation performed in this work was based on first-principles density functional theory (DFT) with planewave basis set and the pseudopotential to describe the electron-ion interactions. The Vienna *ab initio* simulation package (VASP)[33–35] is employed in this study to calculate the electronic structures of the bulk and the low-index surfaces of SnO and SnO_2.

In order to choose a proper pseudopotential, the planewave basis set, and the exchange-correlation functional under generalized gradient approximation (GGA), we made extensive test calculations to optimize the crystal structure of SnO_2 with different pseudopotentials including the projector augmented wave (PAW)[36] and ultrasoft[37,38] methods while for the exchange-correlation functionals we tested both Perdew-Wang (PW91)[39] and Perdew-Burke-Ernzerhof.[40] In the case of Sn pseudopotentials we analyzed both with and without including the $4d$ orbitals of Sn into its pseudopotentials. The results and the corresponding total binding energies per SnO_2 formula unit are listed in Table I.

From Table I we can see that the accuracy of PAW_PW91 is approximately the same as ultrasoft pseudopotential with PW91 exchange-correlation function while including the $4d$ orbitals of Sn in the pseudopotentials. The predicted errors for the crystal structure are similar to those in other calculations.[15] Therefore, in this study, we employ PAW pseudopotential and PW91 exchange-correlation functions in all of the calculations. Plane-wave basis sets are used with a kinetic energy cutoff of 500 eV and an augmentation charge cutoff of 605.4 eV. The k-point sampling grids of $8 \times 8 \times 10$ and $8 \times 8 \times 6$, obtained using the Monkhorst-Pack method,[41] are used for the SnO_2 and SnO bulk calculations, respectively. The k-point sampling grids of $m \times n \times 1$ are used for surface supercell calculations, where m and n are determined by the spacing of around 0.028 Å^{-1} along the a and the b axes of the surface supercell. In the following calculations, we assume all the surfaces have a neutral charge and no extra charge is added in. For bulk calculations, we relax all atoms in the cell. In surface calculations, we fix the middle one to three layers (depending on the symmetry) and let all the other layers relax.

DFT has been very successful in understanding and predicting electronic properties of systems (such as atoms, molecules, and solids) with strong local atom bonds. However, for the sparse systems with both local atom bonds and weak nonlocal van der Waals (vdW) forces between atoms separated by empty space, all practical density functional calculations encounter great difficulty which was shown that

GGA only displays repulsive potential curves with no minimum.[42,43] As shown in the next section, the structure of SnO is layered in the [001] crystallographic direction with a 1/2Sn-O-1/2Sn sequence and a van der Waals gap between two adjacent Sn planes of 2.52 Å.[44,45] Therefore, in order to describe this long range weak vdW interaction between SnO layers, more correlations are needed under DFT-GGA scheme. In the literature, there are several ways to deal with weak vdW interaction.[42,43,46–48] Here we adopted the empirical method, which was proposed by Wu and Yang[42] and has been successfully used to describe vdW characteristics of many systems (such as rare gas,[42] nucleic acid base pairs,[49] water-aromatic interaction,[47] hydrogen-bonded complexes,[48,50] and interlayer binding in graphite[51]), to handle the vdW interaction in the bulk and low-index surfaces of SnO.

For each atom pair separated at a distance R, we add to the density functional electronic structure calculations an additional attraction energy E_{vdW}

$$E_{vdW} = -f_d(R)\frac{C_6}{R^6}, \tag{1}$$

where $f_d(R)$ is the damping function which equals to 1 at large value of R and 0 at small value of R. The C_6 coefficient defines the asymptotic behavior at long range, with its role diminishing at short distances. The E_{vdW} is not a function of electron density, but a function of nuclear positions. As described in Eq. (1), it is independent of DFT calculations and can be calculated very efficiently. The damping function makes it applicable to all cases. For the damping function we take the form of Fermi function

$$f_d(R) = \frac{1}{1 + \exp\left[-\beta\left(\frac{R}{R_m} - 1\right)\right]}, \tag{2}$$

where the R_m is the sum of paired atomic van der Waals radii. The value of β is 23.0.[42] The coefficient C_6 between two atoms A and B can be defined as[24,47]

$$C_6^{A,B} \approx \frac{3}{2}\left[\frac{\alpha^A \alpha^B I_A I_B}{I_A + I_B}\right]. \tag{3}$$

Here α^A and α^B are the dipole polarizabilities of the respective atoms A and B, and the quantities I_A and I_B are the first ionization potentials of the corresponding atoms A and B. By taking the corresponding values of α and I from CRC Handbook,[24] the calculated C_6 coefficients of O-O, Sn-Sn, and Sn-O are 6.569 39, 326.564 87, and 44.194 32 eV Å^6, respectively. The obtained C_6 of O-O is about 5% lower than the value (6.945 03 eV Å^6) reported by Wu and Yang.[42] The van der Waals radii of O and Sn used in this calculation are 1.51 and 2.20 Å, respectively.[24]

Finally, for a given system (bulk or surface), the total binding energy (E_{total}) includes two parts

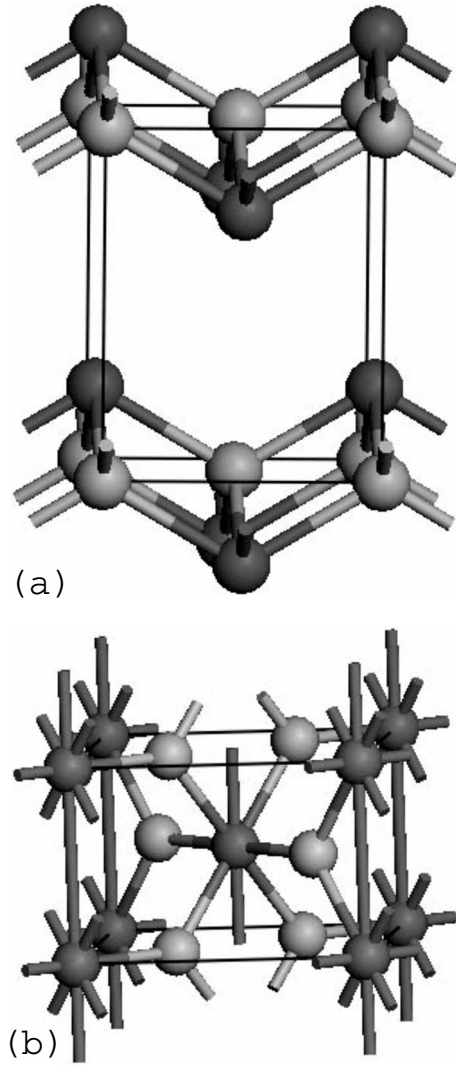$$E_{total} = E_{DFT} + \sum_{i,j} E_{vdW}(R_{i,j}). \tag{4}$$

(a)

(b)

FIG. 1. The optimized crystal structures of SnO (litharge) and SnO$_2$ (rutile). Darker ball stands for Sn and lighter stands for O. (a) SnO, each Sn coordinate with four O atoms and each O is surrounded by four Sn atoms; (b) SnO$_2$, each Sn coordinates with six O atoms and each O is surrounded by three Sn atoms.

The first term (E_{DFT}) comes from the normal DFT calculations with VASP. The second term sums all pairs (atom i and atom j should be located on different layers) in the equilibrium structure optimized by DFT. The actual boundary conditions of the bulk and surfaces should be applied properly during these calculations.

III. RESULTS AND DISCUSSION

A. Bulk SnO and SnO$_2$

1. Geometric parameters of the optimized bulk

Although SnO exists in several different crystal structure forms, experimental and theoretical studies have revealed that the most stable structure for SnO is the litharge,[30,31] whereas the rutile structure is the most stable one for SnO$_2$. Figure 1 shows the crystal structures of SnO and SnO$_2$. The
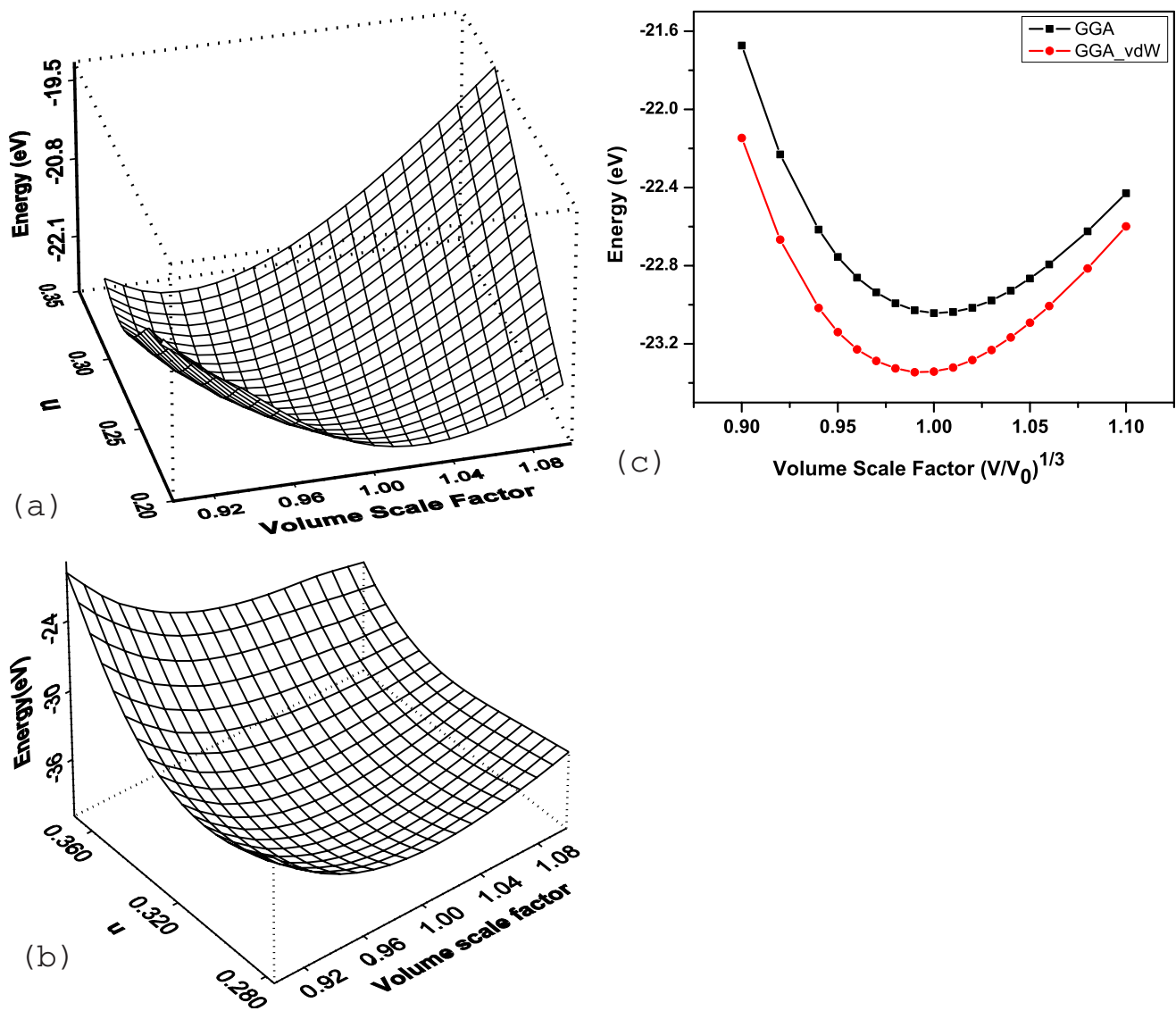
FIG. 2. (Color online) The total binding energy vs cell volume and parameter u for (a) SnO and (b) SnO$_2$. (c) The comparison of binding energy of SnO vs cell volume with and without van der Waals interactions. The volume scale factor is defined as $(V/V_0)^{1/3}$, where V_0 is the equilibrium volume of the cell.

crystallographic space group of SnO in litharge structure is $P4/nmm$ (No. 129) and the lattice constants are $a=b$ $=3.8029$ Å and $c=4.8382$ Å.[44,45] Each Sn and O atom is fourfold coordinated with a bond length of 2.23 Å. The structure is layered in the [001] crystallographic direction with a 1/2Sn-O-1/2Sn sequence and a van der Waals gap between two adjacent Sn planes of 2.52 Å.[1,2,45] In the unit cell, O is at (0,0,0) and (0.5,0.5,0) fractional sites and Sn is located at $(0,0.5,u)$ and $(0.5,0,-u)$ sites with $u=0.2356$. The space group of SnO$_2$ in rutile structure is $P4/mnm$ (No. 136) and the lattice constants are $a=b=4.7373$ Å and $c=3.1864$ Å.[52,53] Each Sn is sixfold coordinated with O while each O atom is threefold coordinated with Sn.[1,2] In the unit cell of SnO$_2$, Sn is located at the corner (0,0,0) and the center (0.5,0.5,0.5), while O is located at $\pm(u,u,0)$ and $\pm(u+0.5,0.5-u,0.5)$ sites with $u=0.307$. It can be seen that the lattice length along the c axis in SnO is close to

the lattice length along the a (or b) axis in SnO$_2$, and vice versa.

In order to explore their bulk properties, with DFT-GGA we calculate the total energy as a function of the cell volume and the relative positions of Sn in SnO and the positions of O in SnO$_2$ by varying parameter u. Figures 2(a) and 2(b) show the calculated total binding energy with the cell volume and the parameter u. With the same amount of variation as shown in Figs. 2(a) and 2(b), it can be found that the binding energy is more sensitive to parameter u than to the cell volume. It is clearly shown that there is a minimum energy valley along the volume change and the position parameter u change. From them, we can obtain the relationship between energy (E) and volume (V) or pressure (P) by fitting the corresponding equation of state. The most popular and well widely used is the Birch-Murnaghan equation of state (E-V). (Refs. 54 and 55),

TABLE II. The fitted parameters of Birch-Murnaghan equation of state for SnO [the experimental crystal constants of SnO (Refs. 44 and 45): $a=b=3.8029$ Å, $c=4.8382$ Å] and SnO_2.

	Method	Optimized structure and error	E_0 (eV)[a]	B_0 (eV/Å³)	B_0'	V_0 (Å³)	Bulk modulus (GPa)	Cohesive energy E_c (eV)
SnO	DFT	$a=3.852$ Å(1.28%) $c=4.969$ Å(2.70%)	−23.04048	0.26448	4.61769	74.66650	42.3 45[b]	9.83 9.6[b]
	DFT+vdW	$a=3.810$ Å(0.19%) $c=4.915$ Å(1.59%)	−23.66816	0.27222	5.19312	71.89616	43.6 45[b]	10.15 9.6[b]
SnO_2	DFT	$a=4.821$ Å(1.78%) $c=3.236$ Å(1.56%)	−37.87513	1.12048	5.02232	75.41359	179.3 218,[b] 138.4[c]	16.17 15.5[b]

[a]The unit cell contains two SnO or SnO_2 units; $E_0/2$ should be used to calculate E_c.
[b]From Ref. 29.
[c]From Ref. 56.

$$E(V) = E_0 + \frac{9 \times B_0 V_0}{16} \left\{ \left[\left(\frac{V_0}{V} \right)^{2/3} - 1 \right]^3 \times B_0' \right.$$
$$\left. + \left[\left(\frac{V_0}{V} \right)^{2/3} - 1 \right]^2 \times \left[6 - 4 \times \left(\frac{V_0}{V} \right)^{2/3} \right] \right\}. \quad (5)$$

By fitting the data of Figs. 2(a) and 2(b) with Eq. (5), we can obtain the parameters in Eq. (5). The fitted results for SnO and SnO_2 are listed in Table II. For SnO, compared to the experimental measurements, the predicted structural constants have 1.28% and 2.70% deviation along the a and c axes which is less than the values of 1.7% and 4.1% obtained by Walsh and Watson,[31] while the deviation of SnO_2 is 1.78% and 1.56% along the a and c axes, respectively (see Table I). It can be seen that for SnO the predicted error along the c axis is higher than that along the a axis. This is due to the van der Waals interaction along the c axis which is not handled well in the DFT scheme.

The bulk modulus B is defined as $B=B_0+B_0' \times P$ in this scheme, where P is the pressure which is set to 1 atm. The optimized equilibrium crystal structures are also listed in Table II. Since our calculating unit cell contains two SnO or SnO_2 formula units, the calculated binding energies of SnO and SnO_2 are −15.52 and −18.94 eV, respectively, which are close to other's reported values.[30] The calculated binding energy difference between SnO_2 and SnO is 1.71 eV/unit which is in good agreement with the XPS experimental value of 1.6 eV.[27] The cohesive energy (E_C) is calculated by subtracting the total bulk energy (E_0 in Table II) from the sum of the total energy of Sn and O atoms using the same level of calculation as we did above for the bulk oxides (in our case, we put the Sn or O atom in the center of $10 \times 10 \times 10$ Å³ box and get $E_{Sn}=-0.6055$ eV and $E_O=-1.0826$ eV). That is $E_C^{SnO_2}=(E_{Sn}+2 \times E_O)-E_{SnO_2}/n$ and $E_C^{SnO}=(E_{Sn}+E_O)-E_{SnO}/n$ where n is the number of SnO or SnO_2 units in the bulk calculations. The calculated E_C as well as other values from references are listed in Table II.

Figure 2(c) shows the binding energy of the SnO bulk vs its cell volume change with and without the vdW interaction correction calculated from Eqs. (1)–(4). From Fig. 2(c), it can be seen that by including the vdW interactions, the fitted equilibrium volume decreases 2.6% compared with the DFT-

GGA only approach. The parameters fitted by the Birch-Murnaghan equation of state Eq. (5) are also listed in Table II. Obviously as shown in Table II, compared to the DFT-GGA-only scheme, the vdW correction yields bulk modulus and structural constants closer to the experimental findings, while the calculated cohesive energy is about 0.55 eV higher than a reported value.[29] As shown in Fig. 1(a) the vdW interaction is along the c axis. Without a correction of the vdW interactions among the SnO layers, the predicted error (2.70%) of the crystal structure constant c is greater than that of the corresponding SnO_2 (1.56% as shown in Table II). After applying the correction of the vdW interactions for SnO, the predicted error drops to 1.59% which gives almost the same precision as in the case of the SnO_2 bulk. These results reveal that the pure DFT-GGA scheme does not fully describe the interacting behavior of the bulk SnO and the precision of the calculation can be improved by including the vdW interactions.

From Table II it also can be seen that our fitted bulk modulus (B) for SnO is quite close to the other reported value,[29] and for SnO_2 the fitted B is lower than some other report,[29] but still reasonable since a different fitting could obtain different values. For example, Camargo et al.[56] obtained a B value of 138.4 GPa. Haines and Leger[57] reported the B value for SnO_2 is between 199 and 208 GPa. Additionally, it should be pointed out that in some fitting procedures the value of B_0' is set to 4.0 and unchanged. In our fitting, we did not apply such constrains and let all the parameters vary. From Table II, one can see that our fitted B_0' is around 5.

2. Electronic structural and thermodynamic properties

From our calculated band structures of SnO and SnO_2, we found that SnO has an indirect band gap of 0.32 eV while SnO_2 has a direct band gap of 0.69 eV which are similar to other calculated results.[32,56,58–60] The calculated band gap of SnO is very close to the recent reported value of 0.3 eV by ab initio FP-LAPW approach.[32] Due to the DFT approximations, which underestimate the excited state energies, the calculated band gaps of the SnO and SnO_2 are smaller than their experimental measurements (2.5–3 eV for SnO and 3.6 eV for SnO_2,[2,61] 0.7 eV for SnO[62]). One possibility for such
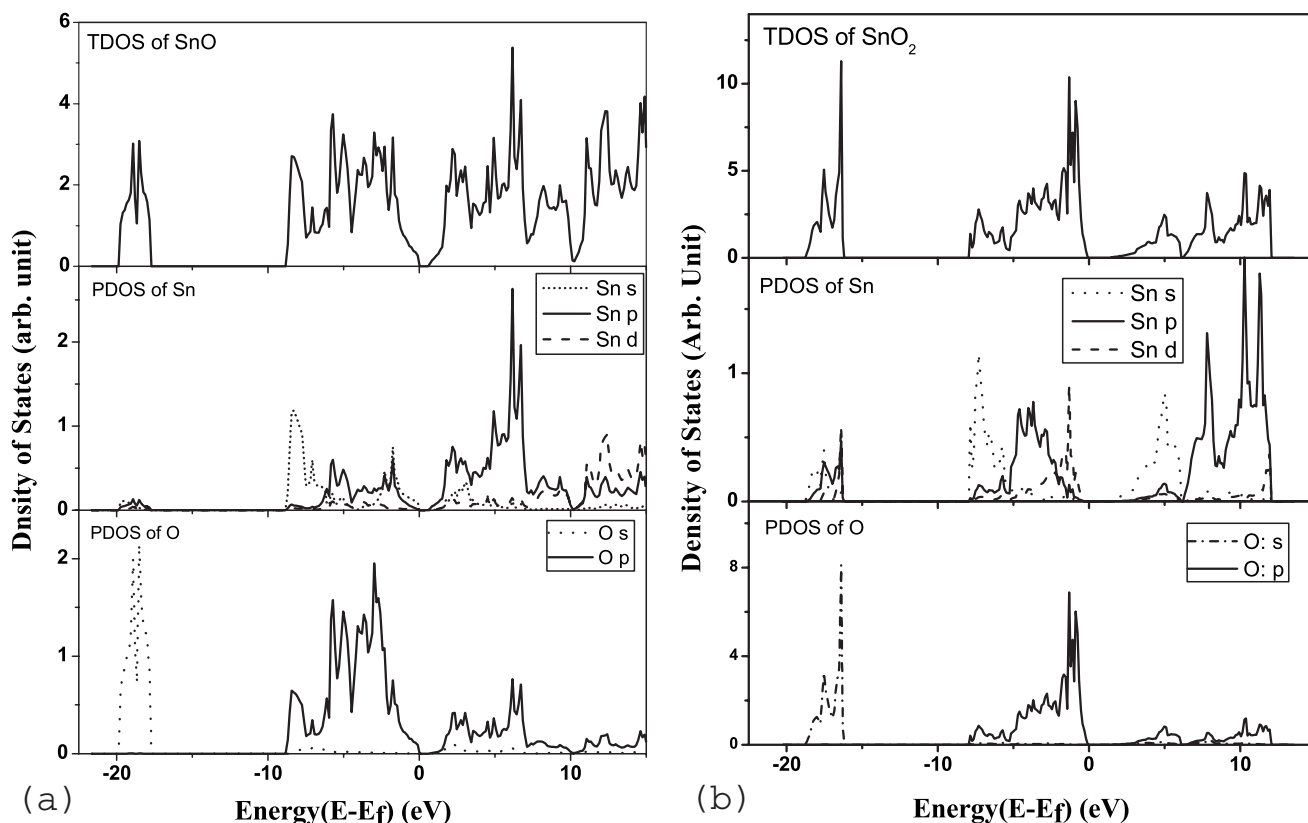
FIG. 3. The calculated density of states of SnO (a) and SnO$_2$ (b). The Fermi level (E_f) is set as relative zero.

large differences is that in tin oxides the correlation effects are large, and the large gaps observed experimentally arise because these oxides are essentially Mott insulators. Christensen *et al.*[63] showed that the band gap width of tin oxide depends sensitively on the c/a ratio. Under the present DFT-GGA approach without other corrections, although different software packages may yield slightly different values (for example, with the CASTEP package the calculated band gap of SnO$_2$ is about 1.15 eV),[64] the calculated band gaps of tin oxides are always smaller than the experimental measurements.[32,56,58–60] There are several ways to correct it: one is to apply the GW method or GGA+U, another is to use so called scissor operation that simply shifts rigidly the unoccupied energy level.[19,58,65] For both SnO and SnO$_2$, their band structures can be divided into two valence bands (VBs) and one conduction band (CB). In both SnO and SnO$_2$, the second VB (below −15 eV) is dominated by O s orbitals. The first VB (0 to−10 eV) and the CB are formed by the O p orbitals with the s, p, and d orbitals of Sn.

Similar to the graphite layer structure, the SnO layers are also mainly bonded by van der Waals interactions. Unlike the sp^2 hybridization of carbon in graphite, in SnO, the Sn and O are hybridized by nonequivalent sp^3 orbitals, where each Sn is bonded by four O and each O is bonded by four Sn atoms. Dissimilar from the C in graphite, there is no unbonded p_z orbital of Sn left in SnO which prevents the semi-metal-like character of the band structure which is found in graphite.

The corresponding total and partial densities of states (TDOS and PDOS) for SnO and SnO$_2$ are shown in Figs. 3(a) and 3(b). From the TDOS shown in Fig. 3, one can see

that both SnO and SnO$_2$ have one very low peak below −15 eV which corresponds to the second VB. The shapes of their first VBs and CBs are different due to the different bonding.

From the PDOS of Sn in SnO shown in Fig. 3(a), one can see that below the Fermi level in the first VB (in the range between 0 and −10 eV) the s orbital of Sn in SnO has a larger contribution than its p and d orbitals and above the Fermi level in the CB the p orbital of Sn has a larger contribution than its s and d orbitals have. The Sn d orbital does not contribute much in the VB and the lower part of its CB. A similar conclusion has also been drawn by Errico's recent reports.[32] However, in Fig. 3(b) of SnO$_2$, comparing it with the case of SnO [Fig. 3(a)], one can see that in the upper part of the first VB the p and d orbitals of Sn play an important role in the formation of this valence band and its s orbital dominates the lower part of the first VB. But in the lower part of its CB, the s orbital of Sn has a larger contribution than its p and d orbitals have. The upper part of its CB is mainly dominated by the p and d orbitals of Sn.

From Fig. 3, one can see that for SnO and SnO$_2$ their PDOS of O are quite similar to each other. The s orbital of O has lower energy and contributes to the second VB below −15 eV and does not take part in chemical bonding with Sn much. The p orbitals of O are involved in the formation of the first VB and the CB. Similar conclusions were also made by Watson,[30] Walsh *et al.*,[31] and Errico.[32] The resonant photoemission for SnO also showed that the O $2p$, Sn $5s$, and Sn $5p$ partial density of states are the main contributors to the valence band.[28]

It has been proven that the Gibbs free energies of solid phases have relatively small variation (<10 meV) in a wide range of temperature (<1500 K) and pressure (<100 atm),[66] as an approximation, we can neglect the zero point energy change and the free energy change of SnO and SnO_2. The chemical potential change $[\Delta\mu(T,P)]$ of the reaction $SnO(s)+0.5O_2(g)\rightarrow SnO_2(s)$ with temperature and pressure dependent is approximated as[67]

$$\Delta\mu(T,P) = \Delta E^0(0,0) + \Delta H_{O_2}(T,p_0) - \frac{1}{2}RT\ln P_{O_2}, \quad (6)$$

where $\Delta E^0(0,0)$ is the energy change between SnO_2 and SnO and O_2 calculated by DFT, and the second term $\Delta H_{O_2}(T,p_0)$, which can be found in the empirical thermodynamic database,[24] is the standard enthalpy of the O_2 gas phase which are contributed from rotations, vibrations, and the ideal-gas entropy at pressure p_0.

With the same calculation approach, we put an O_2 molecule into the center of a $20\times20\times20$ box, the calculated energy of O_2 is -8.7331 eV. The obtained energy change $[\Delta E^0(0,0)]$ for the reaction $SnO(s)+0.5O_2(g)\rightarrow SnO_2(s)$ is -2.737 eV(≈-63.2 kcal/mol). According Eq. (6), at room temperature ($T=298.15$ K), $\Delta H_{O_2}(T,p_0)=0.0$,[24] when $P_{O_2}=1$ atm, the $\Delta\mu(T,P)\approx\Delta E^0(0,0)=-63.2$ kcal/mol which is comparable to the value of -70 kcal/mol calculated from the heats of formation.[2,24] This indicates that the SnO_2 is the thermodynamically most stable form of tin oxides and the reaction is feasible to form SnO_2 from SnO when O_2 is presented. According to Eq. (6), the reverse reaction to dissociate SnO_2 to SnO and O_2 could be occurred when $\Delta\mu(T,P) \geqslant 0$. Obviously, this reverse reaction needs to consume huge amount of energy and therefore is not favorable and only can happen at very high temperature and at very low O_2 pressure. This conclusion agrees with the experimental facts that the SnO_2 can be decomposed into SnO and O_2 starting at 1500 °C.[2]

B. Low-index surfaces of SnO and SnO$_2$

Starting from the optimized equilibrium crystal structures of SnO and SnO_2, for all possible terminations on each low-index surface, we can generate the low-index surfaces which can be stoichiometric or nonstoichiometric. As we pointed out in the Introduction, except for the (111) surface, the stoichiometric low-index surfaces of SnO_2 have been widely investigated in the literature.[2,7,8,14,68,69] Here in this study, we are focusing on the surfaces of SnO and the (111) surface of SnO_2. For comparison, the results of other stoichiometric surfaces of SnO_2 are also presented when necessary.

To generate the surface slab from the bulk, we either keep both surfaces of the slab identical or after performing translation or inverse symmetry on the surface plane they become the same, after which we can cleave atoms layer by layer to obtain different terminations. In this way the generated surfaces are nonpolar. With this constraint, for some surfaces [such as (001), (100), and (011)], we can only generate the stoichiometric slab in which both surfaces are the same. For some other surfaces [such as (110) and (111)] we can generate both stoichiometric and nonstoichiometric slabs (see the

following subsections). It should be pointed out that without the constraint of both surfaces of the slab being the same we can get more surface slabs for different terminations than those presented in this work. However, in that way, some of them are mixed polar surfaces, in which both surfaces of the slab are not the same. Therefore, in this work, all generated surface slabs are symmetric (which means both surfaces are the same) and can be stoichiometric or nonstoichiometric. All surfaces are generated by the Accelrys' MATERIALS STUDIO 4.1 software package.

Following the above procedure, all possible symmetrical stoichiometric low-index surfaces of SnO and (111) surfaces of SnO_2 are generated and shown in Fig. 4. For comparison, the stable low-index symmetric stoichiometric surfaces of SnO_2 are also shown in Fig. 4. Figure 5 shows all possible symmetrical nonstoichiometric low-index surfaces of SnO and (111) surface of SnO_2. Comparing Fig. 4 with Fig. 5 one can see that only (110) and (111) low indices of SnO and (111) index of SnO_2 can have symmetric nonstoichiometric surfaces [except for (111) surface, we did not apply this procedure to other low-index surfaces of SnO_2]. Since in this work we are investigating the pure clean surface, these surfaces can be represented by a 1×1 surface. As we discuss in the next subsection, the number of layers does affect the calculation precision, the actual number of layer in our calculations ($\geqslant6$) is more than the layers shown in Figs. 4 and 5 where less layers and more than one unit cell along the surface are presented just for display purposes.

For stoichiometric surfaces, usually the surface energy (E_{surf}) can be defined as the energy of the surface slab related to its bulk reference:[1,2,7,8,13,16,70]

$$E_{surf} = \frac{E_{slab} - nE_{bulk}}{2A}, \quad (7)$$

where E_{slab} is the total energy of the surface slab, E_{bulk} is the total energy of the bulk material SnO or SnO_2, A is the surface area with a factor of 2 due to each slab containing two surfaces, and n is the number of SnO or SnO_2 formula units in the slab. From our calculations, $E_{bulk}(SnO)=-11.521$ eV, and $E_{bulk}(SnO_2)=-18.942$ eV.

For the nonstoichiometric symmetric surface slab, there is no standard definition for the surface energy. Here, we follow the thermodynamic formalism proposed by Reuter and Scheffler[71] to calculate the surface free energy $\gamma(p,T)$, which can be applied for both stoichiometric and nonstoichiometric surfaces. Considering a surface in contact with oxygen atmosphere described by an oxygen pressure p and temperature T, the appropriate thermodynamic potential required to describe such a system is the Gibbs free energy $G(T,p,N_{Sn},N_O)$ where N_{Sn} and N_O are the number of Sn and O atoms in the sample. The most stable surface composition and geometry is then the one that minimizes the $\gamma(p,T)$, defined as

$$\gamma(p,T) = \frac{1}{2A}[G^{slab}(p,T,N_{Sn},N_O) - N_{Sn}\mu_{Sn}(p,T)$$
$$- N_O\mu_O(T,p)], \quad (8)$$

where $\mu_{Sn}(p,T)$ and $\mu_O(p,T)$ are the chemical potentials of a
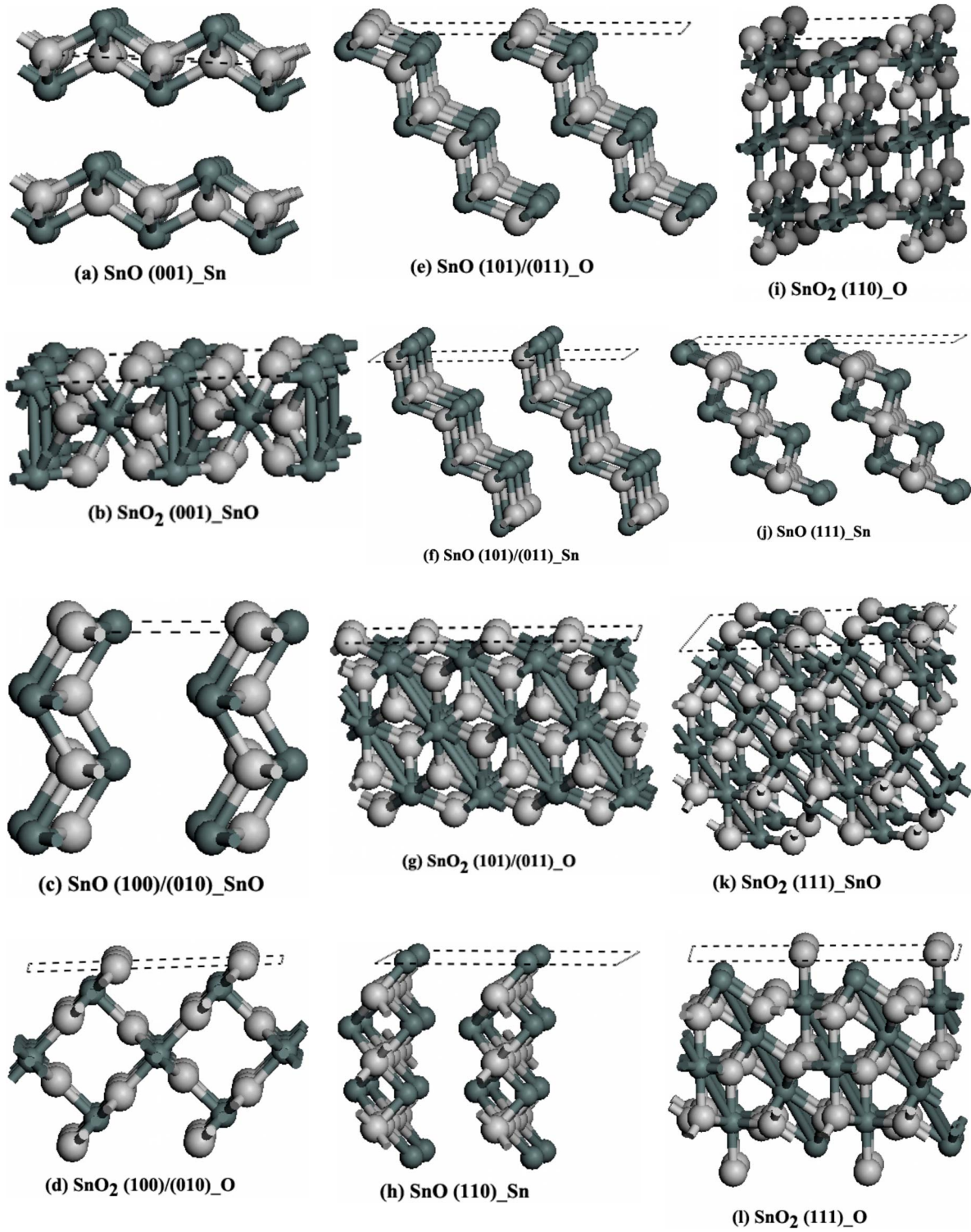
FIG. 4. (Color online) The low-index symmetrical stoichiometric surfaces of SnO and SnO$_2$. Darker balls represent the Sn atoms while brighter balls the O atoms. Notations _O, _Sn, and _SnO correspond to O, Sn, and mixed O and Sn terminations, respectively.

Sn and an O atom, and can be related by the Gibbs free energy of the bulk SnO$_2$ and SnO $\left[g^{\text{bulk}}(p,T)\right]$

$$\mu_{\text{Sn}}(p,T) + 2\mu_{\text{O}}(p,T) = g^{\text{bulk}}_{\text{SnO}_2}(p,T), \qquad (9a)$$

$$\mu_{\text{Sn}}(p,T) + \mu_{\text{O}}(p,T) = g^{\text{bulk}}_{\text{SnO}}(p,T). \qquad (9b)$$

Inserting Eqs. (9a) and (9b) into Eq. (8) leads to

$$\gamma_{\text{SnO}_2}(p,T) = \frac{1}{2A}\left[G^{\text{slab}}_{\text{SnO}_2}(p,T,N_{\text{Sn}},N_{\text{O}}) - N_{\text{Sn}}g^{\text{bulk}}_{\text{SnO}_2}(p,T)\right.$$
$$\left. + (2N_{\text{Sn}} - N_{\text{O}})\mu_{\text{O}}(T,p)\right], \qquad (10a)$$
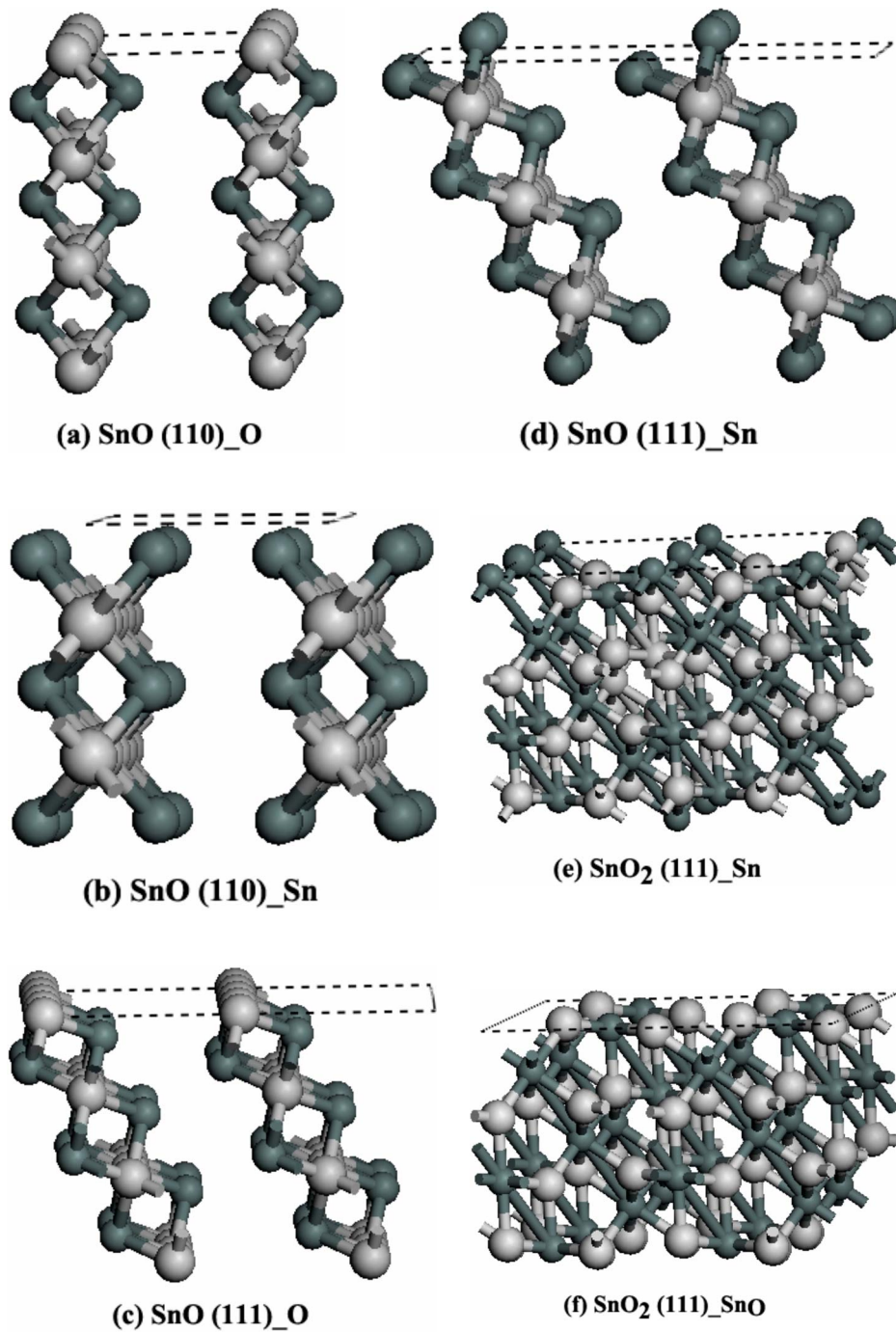
FIG. 5. (Color online) The low-index symmetrical nonstoichiometric surfaces of SnO and the (111) surfaces of SnO$_2$. Darker balls represent Sn atoms while brighter balls the O atoms.

$$\gamma_{\text{SnO}}(p,T) = \frac{1}{2A}[G_{\text{SnO}}^{\text{slab}}(p,T,N_{\text{Sn}},N_{\text{O}}) - N_{\text{Sn}}g_{\text{SnO}}^{\text{bulk}}(p,T)$$

$$+ (N_{\text{Sn}} - N_{\text{O}})\mu_{\text{O}}(T,p)]. \qquad (10b)$$

The Gibbs free energy of formation (ΔG_f) of SnO$_2$ and SnO are defined as

$$\Delta G_f^{\text{SnO}_2}(p,T) = g_{\text{SnO}_2}^{\text{bulk}}(p,T) - g_{\text{Sn}}^{\text{bulk}}(p,T) - g_{\text{O}_2}^{\text{gas}}(p,T),$$

$$(11a)$$

$$\Delta G_f^{\text{SnO}}(p,T) = g_{\text{SnO}}^{\text{bulk}}(p,T) - g_{\text{Sn}}^{\text{bulk}}(p,T) - \tfrac{1}{2}g_{\text{O}_2}^{\text{gas}}(p,T),$$

$$(11b)$$

where $g_{\text{O}_2}^{\text{gas}}(p,T)$ is the Gibbs free energy of an O$_2$ molecule and $g_{\text{Sn}}^{\text{bulk}}(p,T)$ is the Gibbs free energy of the bulk tin. The range of oxygen chemical potential is

$$\tfrac{1}{2}\Delta G_f^{\text{SnO}_2}(0,0) < \mu_{\text{O}}(p,T) - \tfrac{1}{2}E_{\text{O}_2}^{\text{total}} < 0 \quad (\text{SnO}_2),$$

$$(12a)$$

$$\Delta G_f^{SnO}(0,0) < \mu_O(p,T) - \tfrac{1}{2}E_{O_2}^{total} < 0 \quad \text{(SnO)}, \quad (12b)$$

where $E_{O_2}^{total}$ is the total energy of a free, isolated O_2 molecule at $T=0$ K. The calculated $E_{O_2}^{total}$, $\Delta G_f^{SnO_2}(T \to 0 \text{ K}, 1 \text{ atm})$, and $\Delta G_f^{SnO}(T \to 0 \text{ K}, 1 \text{ atm})$ are -8.733, -6.342, and -3.288 eV, respectively. This range gives the upper and lower bounds of $\mu_O(p,T)$ which refer to O-rich and O-poor limits.

Obviously, as an approximation, for the calculated total energy (E_{bulk}, E_{slab}) one can substitute the Gibbs free energy (g^{bulk}, G^{slab}) in Eqs. (10a) and (10b) by neglecting zero vibrations and temperature. The surface free energy $\gamma(p,T)$ is a function of the oxygen chemical potential. In the case of stoichiometric surfaces, the surface free energy only depends on the total energy (E_{bulk}, E_{slab}) and Eqs. (10a) and (10b) are simplified to the traditional surface energy definition (7).[13,14]

1. Effects of slab thickness

In order to explore how many layers are needed to represent the surface slab and to obtain reasonable results, we calculated the surface energy for different numbers of layers of slab. In order to remove the effects of the vacuum size added in our slab to form the supercell, we kept the volume of supercell unchanged by adjusting the size of vacuum (with a minimum of 10 Å) for different layer systems. As an example, Figs. 6(a) and 6(b) show the relation between surface energy and the number of layers in the SnO and SnO_2 slabs, respectively.

From Fig. 6 one can see that the surface energy varies with the number of layers in the slab. When the number of layers is 5 or higher, the surface energies start to converge to a constant value. Therefore, for the surface calculation, in order to achieve reliable results, the number of layers should be greater than 5. Bates *et al.*[70] investigated the energetic relationship of slab thickness for $TiO_2(110)$ and obtained a similar conclusion, namely, that at least six layers are necessary to achieve similar convergence of the surface energy. Bergermayer and Tanaka[9] concluded that a five layer slab for the (110) SnO_2 surface and a seven layer slab for the (101) SnO_2 surface with a vacuum of 10 Å are sufficient to obtain results with convergence in E_{surf} within 5 meV/Å. In the following calculations, we generate the surface with at least six layers. The exact number of layers for different index surfaces is given in the following subsections.

Like bulk calculations, the surface system is also treated with the periodic boundary condition and neutral charge. We also examined the effects of the size of vacuum added to the SnO_2 (110) surface slab to form the supercell. Our results show that increasing the vacuum size can lead to a little bit lower surface energy. Compared with the vacuum size $(Lv) =10$ Å added into the same SnO_2 (110) surface slab, the total binding energy changes are 0.019, -0.007, -0.010, and -0.013 eV for $Lv=5$, 20, 30, and 40 Å, respectively. In our following calculations, we typically set the vacuum size for all surface slabs to at least 10 Å to obtain reliable results.

2. (001) surface

The (001) surface of SnO is shown in Fig. 4(a), which is a stoichiometric surface with Sn on top. The O is located in
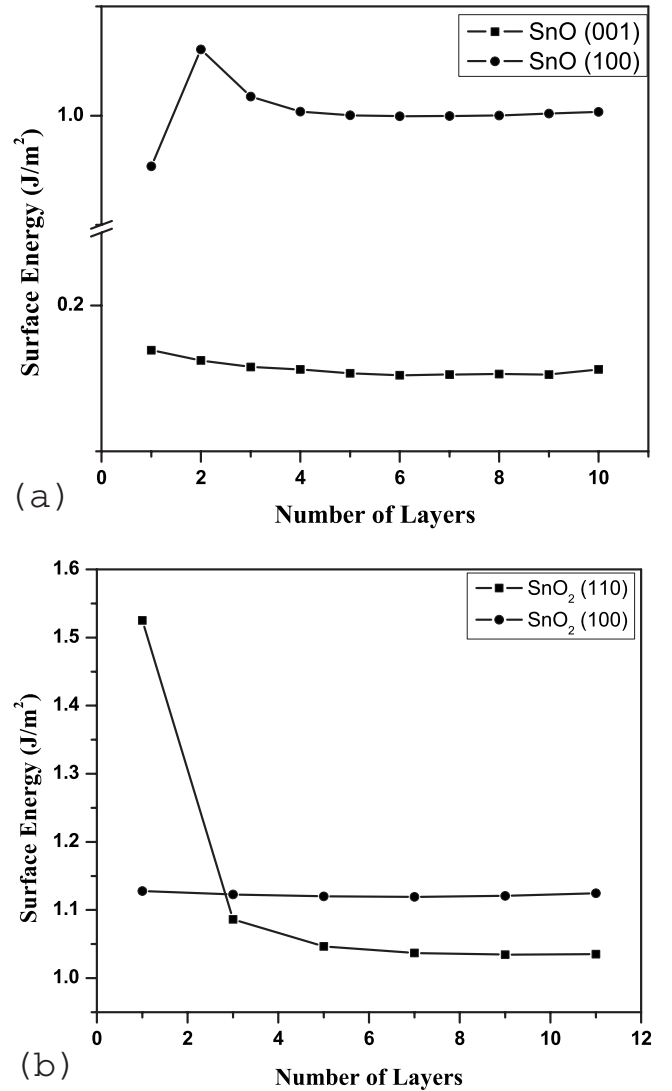

(a)

(b)

FIG. 6. The variation of the surface energy with number of layers in the slab. (a) the (001) and (100) surfaces of SnO [see Figs. 4(a) and 4(c)], (b) the (110) and (100) surfaces of SnO_2 [see Figs. 4(i) and 4(d)].

the valley between Sn atoms. However, for the (001) surface of SnO_2, both Sn and O are on the surface [see Fig. 4(b)]. The generated (001) 1×1 surface slabs of SnO and SnO_2 contain $Sn_{14}O_{14}$ and $Sn_{13}O_{26}$ with 14 and 13 layers of Sn, respectively.

With Eq. (7), we can calculate the surface energies of the (001) surfaces of SnO [Fig. 4(a)] and SnO_2 [Fig. 4(b)]. The results obtained are 0.081 and 1.872 J/m^2, respectively. Obviously, the SnO_2 (001) surface has a much higher surface energy than the SnO (001) surface does. Therefore, the SnO (001) surface is more stable than the SnO_2 (001) surface. Comparing Fig. 4(a) with Fig. 4(b), one can see that on the (001) surface of SnO only Sn atoms are on the surface and their valence is already saturated. Comparing Fig. 4(a) with Fig. 1(a), it is clear that in order to form the (001) surface of SnO only the van der Waals interactions between two adjacent Sn planes are broken and these kinds of interactions are normally weaker compared to the chemical bonding. How-
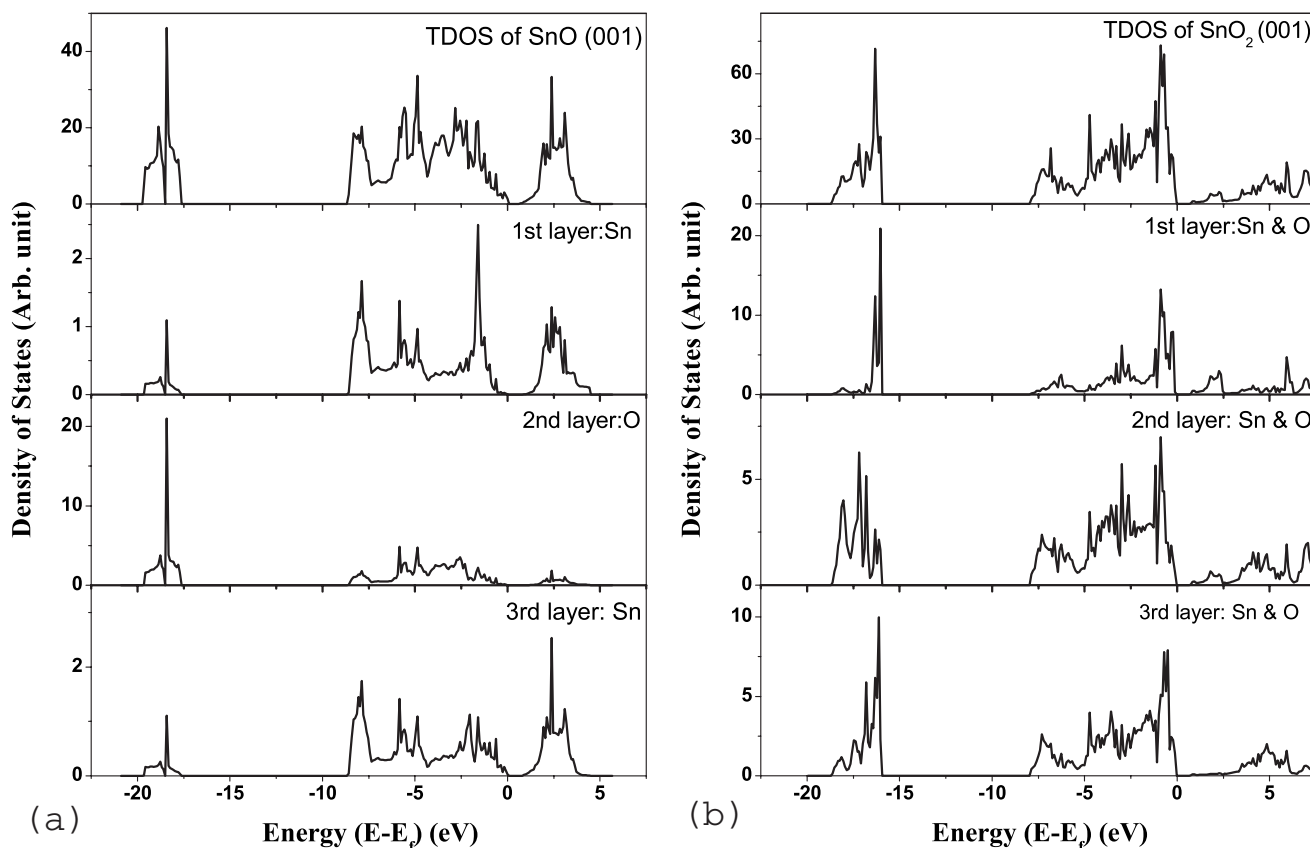
FIG. 7. The total and layer resolved partial density of states of the (001) surfaces of SnO (a) and SnO$_2$ (b).

ever, in the case of SnO$_2$, in order to form its (001) surface there are several chemical bonds for both Sn and O on the surface layer that need to be broken, which results in a higher surface energy.

The calculated TDOS of the (001) surface slab and the PDOS of the top three layers of SnO and SnO$_2$ are shown in Fig. 7. Comparing the TDOS of the (001) surface shown in Fig. 7 with the TDOS of bulk SnO and SnO$_2$ shown in Fig. 3, it can be seen that the big differences are around the Fermi level. In the case of the SnO (001) surface shown in Figs. 7(a) and 4(a), the top layer is Sn, and the second and third layers are O and Sn, respectively. The surface state is dominated mainly with the 5s and 5p orbitals of the first layer of Sn and the 2p orbitals of the second layer of O. The PDOS of the first layer of Sn and the third layer of Sn are quite different because the first layer of Sn forms the surface state and the behavior of the third layer of Sn is more like the Sn in the bulk. However, in the case of the SnO$_2$ (001) surface shown in Figs. 7(b) and 4(b), the surface layer contains both Sn and O just like its bulk. Although the PDOS of each layer is different due to the formation of the surface state, from the first to third layer, its PDOS is becoming similar to its bulk DOS as shown in Fig. 3(b).

3. (100) or (010) surface

For SnO and SnO$_2$, their (100) and (010) surfaces are identical. For SnO there is only one type of termination for the (100) or (010) surface which is stoichiometric and is

shown in Fig. 4(c). Unlike its (001) surface as shown in Fig. 4(a), each layer of this type of surface contains both O and Sn. The surface is perpendicular to each slice of SnO. Along the ⟨100⟩ direction (which in the figure is horizontal) there are parallel repeats of Sn-O slices. These slices are mainly bonded to each other by weak van der Waals interactions. Therefore, this surface should have higher surface energy and be less stable compared to its (001) surface. Compared with SnO, the (100) surface of SnO$_2$ could have several different terminations and several possible stoichiometric or nonstoichiometric surfaces. However, as pointed out by other researchers,[1,8,14] the one with the O termination is the most stable (100) surface as shown in Fig. 4(d). Similar to the (001) surface, the generated (100) or (010) 1×1 surface slabs of SnO and SnO$_2$ are Sn$_{10}$O$_{10}$ and Sn$_{11}$O$_{22}$ with 10 and 11 layers of Sn, respectively.

The calculated E_{surf} of the SnO (100) surface is 0.39 J/m^2, which is higher than its (001) surface (0.081 J/m^2). On the SnO$_2$ (100) surface, the O in Fig. 4(c) is on the top layer and its valence is not saturated, thus it can interact with other molecules easily. Therefore, it is not surprising that the SnO$_2$ (100) surface has higher surface energy (1.128 J/m^2) than the SnO (100) surface does.

The calculated TDOS of the (100) surfaces and PDOS of the first three layers of SnO and SnO$_2$ are shown in Fig. 8. From Figs. 4(c) and 8(a), it can be seen that in the SnO (100) or (010) surface each layer contains both Sn and O. The PDOS of the top layer has some differences compared with the inner second and third layers because on the top layer Sn
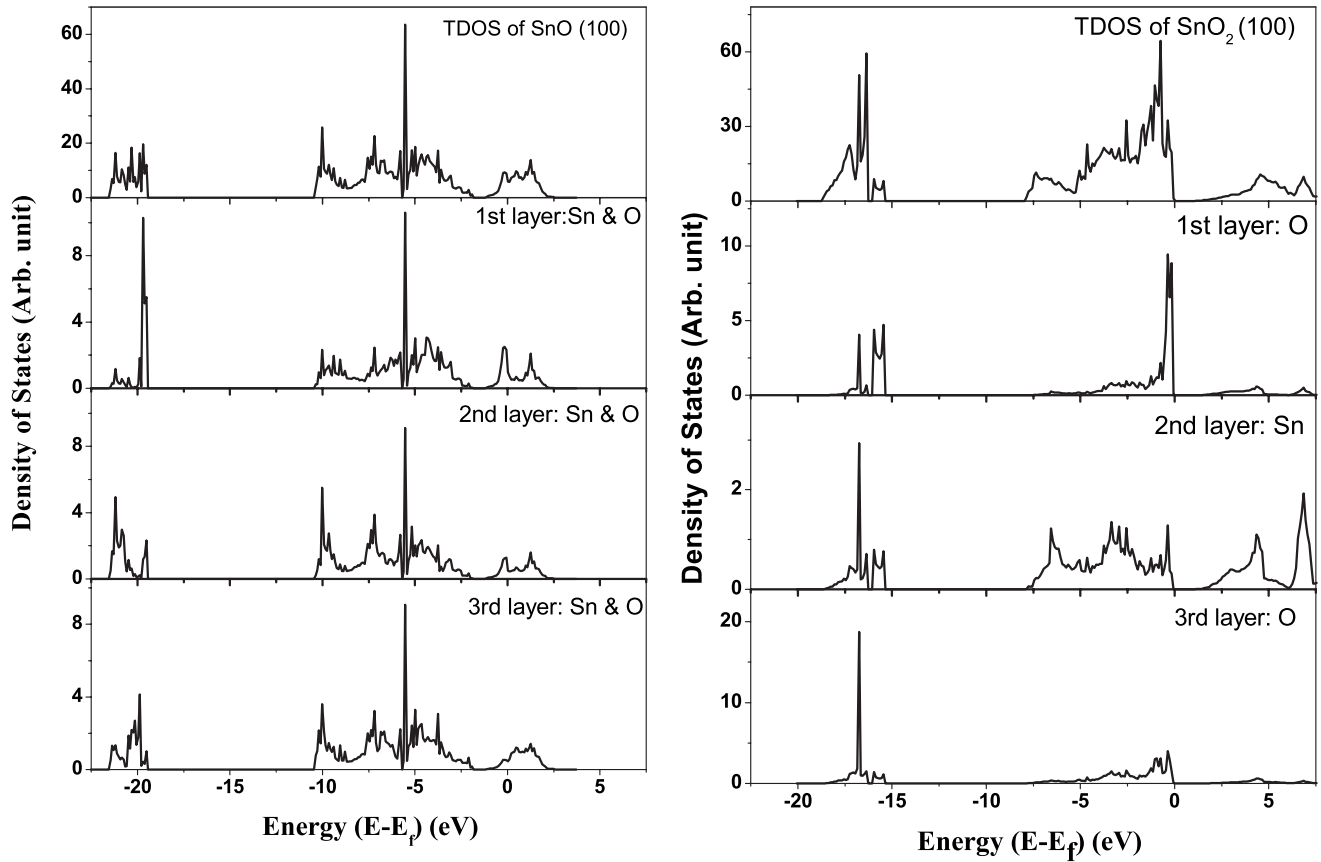
FIG. 8. The total and layer resolved partial density of states of the (100) or (010) surfaces of SnO (a) and SnO_2 (b).

and O are threefold bonded whereas in the inner layer they are fourfold bonded to each other. In Figs. 4(d) and 8(b), the SnO_2 (100) or (010) surface terminates with O, the second layer is Sn, and the third layer is O again. From the PDOS of these three layers shown in Fig. 8(b), it can be seen that the bonding in the first layer of O is different from that in the third layer of O because on the top layer the O is twofold bonded where in the inner layer it is threefold bonded.

4. (101) or (011) surface

Just as the (100) and (010) surfaces, the (101) and (011) surfaces of SnO and SnO_2 are the same. From its optimized bulk structure we can generate two kinds of low-index surface slab for SnO in which O or Sn is on the top layer. These two kinds of surfaces are stoichiometric as shown in Figs. 4(e) and 4(f). In both cases, the top O in Fig. 4(e) and the top Sn in Fig. 4(f) are threefold bonded which is different from their coordination in bulk where both O and Sn are fourfold bonded with each other. From Figs. 4(e) and 4(f) it can be seen that the distance between the first two layers is much shorter than the distance between the second and third layers. Compared to its (100) surface shown in Fig. 4(c), it can be seen that the structural patterns have some similarities, but their atom arrangements on each layer are not the same and the repeat unit along *b* direction in the (101) surface is larger than that in the (100) surface. Unlike in the (100) surface, the O and Sn in the (101) surface slab are not on the same plane. The stable stoichiometric (101) surface for SnO_2 is also

shown in Fig. 4(g) in which the O terminated on the top layer.

Similar to their (100) surfaces, the generated (101) or (011) 1×1 surface slabs of SnO and SnO_2 are $Sn_{10}O_{10}$, $Sn_{10}O_{10}$, and $Sn_{12}O_{24}$ with ten, ten, and six layers of Sn respectively. The calculated surface energies (see Table III) show that the O terminated surface [Fig. 4(e)] has a little bit lower E_{surf} than the Sn-terminated surface [Fig. 4(f)] by 0.06 J/m^2. This is because the dangling bonds of O in Fig. 4(e) are less than that of Sn in Fig. 4(f). Therefore, the O-terminated surface in Fig. 4(e) is more stable than the Sn-terminated surface in Fig. 4(f). Comparing the SnO_2 (101) surface shown in Fig. 4(g) with the SnO (101) surfaces, one can see that on the SnO_2 (101) surface the O is on the top and the Sn is on the second layer. However, the second layer of Sn is still exposed to the surface between the first layer of O. Therefore, the second layer of Sn also contributes to the surface and possible acts as active sites.

In Fig. 9 are given the TDOS of SnO and SnO_2 (101)/(011) surfaces and PDOS of their top three layers. Comparing the TDOS of the bulk SnO in Fig. 3(a) with the TDOS of its (101) surfaces in Figs. 9(a) and 9(b), it can be seen that the surface states are located around the Fermi level. In the case of the O-terminated (101) surface [Figs. 4(e) and 9(a)], the PDOS of the second layer of Sn is quite different from that of the third layer of Sn, which means that the second layer of Sn is strongly involved in surface state formation. Although the distance between the third layer and the second layer is quite small as shown in Fig. 4(e), the

TABLE III. The calculated surface energy for SnO and SnO$_2$ (J/m^2).

Surfaces		(001)	(010)/(100)	(101)/(011)	(110)	(111)
SnO	DFT	0.081[a]	0.390[b]	0.407,[a] 0.347[c]	0.503[a]	0.527[a]
	DFT+vdW	0.184[a]	0.445[b]	0.507,[a] 0.454[c]	0.564[a]	0.810[a]
SnO$_2$	DFT	1.871[b]	1.128[c]	1.461[c]	1.035[c]	2.071,[b] 1.887[c]
		1.84,[d] 1.72,[e] 1.74[f]	1.27,[d] 1.14,[e] 0.92[f]	1.43,[d] 1.33,[e] 1.28[f]	120,[d] 1.04,[e] 1.01[f]	2.217[g]

[a]Sn-terminated surface.
[b]Both Sn- and O-terminated surface.
[c]O-terminated surface.
[d]From Ref. 73.
[e]From Ref. 14.
[f]From Ref. 2.
[g]From Ref. 12.

third layer of Sn is far from the top O compared to the second layer of Sn, which results in weaker interactions and less contributions to the surface states. A similar conclusion can also be drawn for the case of the Sn-terminated (101) surface of SnO [Figs. 4(f) and 9(b)] in which the second layer of O is strongly involved in surface state formation compared to the third layer of O. In the case of the SnO$_2$ (101) surface, both the first layer of O and the second layer of Sn are involved in forming the surface state. Both TDOS and PDOS of SnO (101) surfaces are quite different from those of SnO$_2$ (101) surfaces [Figs. 4(g) and 9(c)], which is due to the different structures and bonding. As one can see that the bonding in the SnO$_2$ (101) surface is much stronger than that in the SnO (101) surfaces, where the latter has van der Waals interactions between the slices. The relative intensities of their DOS, given in Fig. 9, also show this feature.

5. (110) surface

Compared with other low-index surfaces of SnO$_2$, its (110) surface has been intensively investigated both in experimental and theoretical studies,[6,7,14–16,18,58,72] and it has been proved that this surface is the most stable one with the lowest surface energy. Our calculated results also reach the same conclusion (see Table III for details). The structure of the SnO$_2$ (110) surface is shown in Fig. 4(i) in which the O is on the top layer and between the O's there is a large gap which exposes the second layer O and Sn.

As for SnO, from its optimized bulk structure, three possible (110) symmetrical surfaces can be obtained as shown in Fig. 4(h), and Figs. 5(a) and 5(b), respectively. Strictly speaking, it is impossible to generate a stoichiometric symmetrical (110) surface of SnO by simply cleaving surface atoms layer by layer. The one shown in Fig. 4(h) is obtained in a different manner by cleaving half of the Sn on the surface layer of Fig. 5(b). This surface has Sn-O-Sn repeating layers parallel to the surface. Figures 5(a) and 5(b) are two possible symmetric nonstoichiometric (110) surfaces of SnO that within the SnO (110) surface slabs the Sn-O slices are arranged in parallel. Among these slices, only van der Waals interactions bind them together. On the surface, either O or Sn twofold binds with Sn or O which is different from its bulk in which both O and Sn are fourfold bonded. The generated (110) 1×1 surface slabs of SnO are Sn$_{12}$O$_{12}$, Sn$_{10}$O$_{12}$, and Sn$_{12}$O$_{10}$ with seven, five, and six layers of Sn and six, six, and five layers of O, respectively.

However, the generated (110) 1×1 surface slab of SnO$_2$ is Sn$_{10}$O$_{20}$ with six layers of Sn. The calculated surface energies of the (110) stoichiometric surfaces of SnO and SnO$_2$ as shown in Figs. 4(h) and 4(i) are 0.503 and 1.054 J/m^2, respectively. Although among the low-index surfaces of SnO$_2$, the (110) surface is the most stable one, when comparing that with the (110) surface of SnO one can see that the surface energy of SnO (110) is even lower than that of the SnO$_2$ (110) surface.

To deal with the symmetrical nonstoichiometric surfaces [Figs. 5(a) and 5(b)], following Eqs. (10b), (11b), and (12b) the surface free energies [$\gamma(p,T)$] are calculated with the different oxygen chemical potentials [$\mu_O(p,T)$]. Figure 10 shows the relationship between $\gamma(p,T)$ and $\mu_O(p,T)$ of the (110) surfaces of SnO. In our case, the condition is $p=1$ atm, $T \rightarrow 0$ K.

From Fig. 10, one can see that the $\gamma(p,T)$ of the stoichiometric (110) surface is the same as its E_{surf} calculated from Eq. (6) and remains unchanged with a varying $\mu_O(p,T)$. The $\gamma(p,T)$ of the Sn-terminated nonstoichiometric (110) surface of SnO [Fig. 5(b)] increases with increasing $\mu_O(p,T)$. During the whole range of $\mu_O(p,T)$ it is greater than the $\gamma(p,T)$ of the corresponding stoichiometric surface, which means this kind of nonstoichiometric surface [Fig. 5(b)] is unstable. However, for the O-terminated nonstoichiometric surface as shown in Fig. 5(a), its $\gamma(p,T)$ decreases when the $\mu_O(p,T)$ change from O poor to O rich and when $\mu_O(p,T)$ close to reach O-rich bound the $\gamma(p,T)$ of this surface is lower than the corresponding stoichiometric ones, which means under O-rich condition with higher $\mu_O(p,T)$ this surface could become more stable than the corresponding stoichiometric surface.

In Fig. 11 are shown the TDOS of the (110) surfaces of SnO and SnO$_2$. From the TDOS of the SnO nonstoichiometric (110) surfaces shown in Figs. 11(a) and 11(b), it can been seen that these two surfaces are quite different. For the Sn-terminated (110) surface [Fig. 11(b)], there is no gap between the first VB and the CB (precisely at Γ point). Comparing to O-terminated surface as shown in Fig. 11(a), its CB is shifted to the valence band side. In the case of the O-terminated (110) surface of SnO, the s orbital of the second layer of Sn also has some contributions to the lowest VB, whereas in the case of the Sn-terminated (110) surface it only has a relative small contributions. Therefore, the Sn-terminated surface should have higher surface energy than
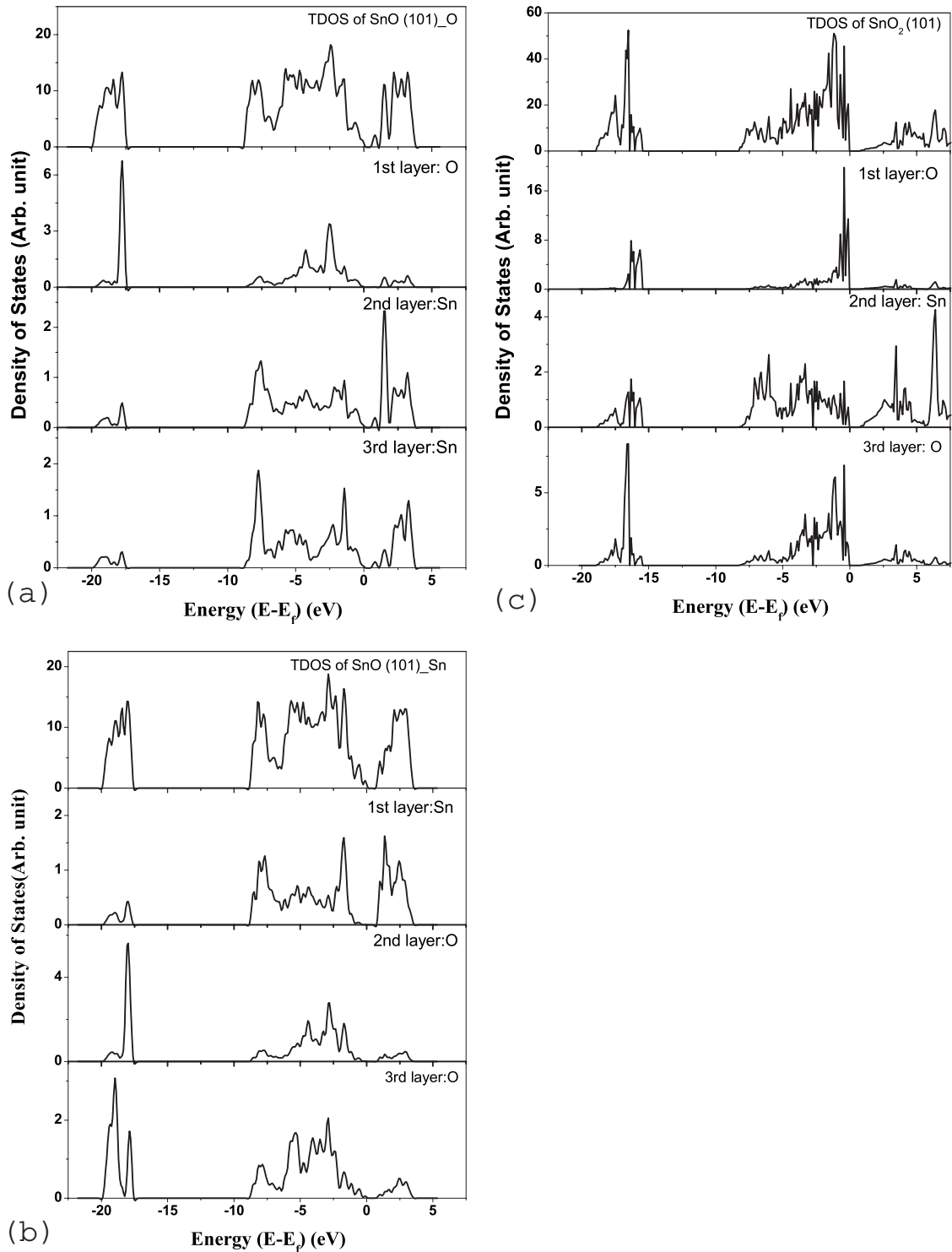
FIG. 9. The total and layer resolved partial density of states of the (101) or (011) surfaces of SnO and SnO$_2$. (a) O-terminated SnO (101) surface, (b) Sn-terminated SnO (101) surface, and (c) O-terminated SnO$_2$ (101) surface.

the O-terminated surface. From the TDOS of the stoichiometric (110) surface of SnO as shown in Fig. 11(c), it can be seen that there is an obvious gap between the first VB and the CB. The TDOS of the SnO$_2$ (110) surface is shown in Fig. 11(d). From their PDOS (not shown in the figure) the surface states are dominated by the first layer of O and the second layer of O and Sn because the PDOS of the third

layer of O is similar with that in its bulk [Fig. 3(b)].

6. (111) surface

Only three different types of SnO (111) symmetrical surfaces can be obtained from its optimized bulk and are shown in Fig. 4(j) and Figs. 5(c) and 5(d). Both Figs. 5(c) and 5(d) are nonstoichiometric surfaces while Fig. 4(j) is a stoichio-
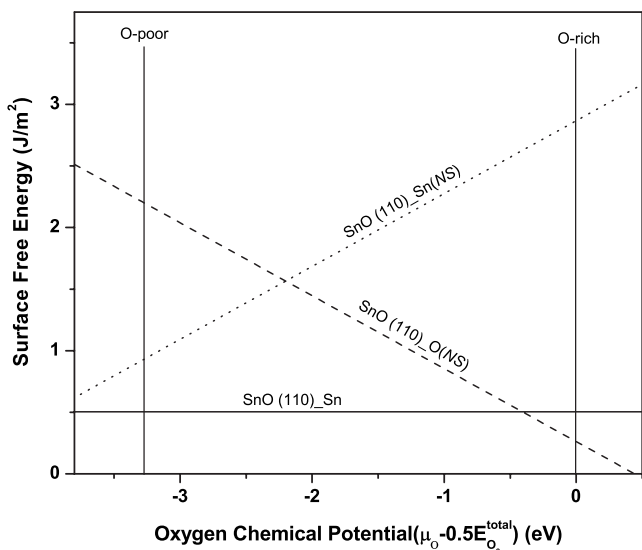
FIG. 10. The surface free energy of the (110) surface of SnO versus the oxygen chemical potentials. The NS labeled in the figure stands for nonstoichiometric.

FIG. 11. The total density of states of the (110) surfaces of SnO and SnO_2. (a) The O-terminated nonstoichiometric (110) surface of SnO, (b) the Sn-terminated nonstoichiometric (110) surface of SnO, (c) the Sn-terminated stoichiometric (110) surface of SnO, and (d) the O-terminated (110) surface of SnO_2.

metric one. Unlike other low-index surfaces, the repeat unit of these surfaces is not a rectangle, but a hexagonal with the angle between a axis and b axis of 116°. Comparing to its (110) surface as shown in Fig. 4(h), one can see that their patterns of atom arrangements are much similar to each other. However, the distances between atoms are not the same. Unlike the (110) surfaces, the (111) surface has a larger size of repeat unit cell and are not rectangle, the repeat layer is in the pattern of [O-Sn-Sn-O] and the Sn atoms are not on the same plane. The generated (111) 1×1 surface slabs of SnO are $Sn_{12}O_{12}$, $Sn_{12}O_{14}$, and $Sn_{14}O_{12}$ with 12, 12, and 14 layers of Sn and 6, 7, and 6 layers of O, respectively.

The (111) surface of SnO_2 has not attracted researchers' too much interests and is rarely studied. Using ionic model, Mulheran and Harding[12] investigated the stability of a number of SnO_2 surfaces. From their calculated excess energy per unit cell (ΔE), they concluded that the (110) surface is the most stable surface with $\Delta E = 1.380$ J/m^2 and the (111) surface is the second unstable surface with $\Delta E = 2.217$ J/m^2. Surprisingly, the most unstable surface for SnO_2 they predicted is (001) with $\Delta E = 2.366$ J/m^2.

Starting from the optimized equilibrium crystal structure of SnO_2 as shown in Fig. 1(b), four possible symmetric (111) surfaces of SnO_2 are generated and shown in Figs. 4(k), 4(l), 5(e), and 5(f), respectively. The generated (111) 1×1 surface slabs of SnO_2 are $Sn_{17}O_{34}$, $Sn_{13}O_{26}$, $Sn_{13}O_{24}$, and $Sn_{17}O_{36}$ with 17, 13, 13, and 17 layers of Sn and 24, 20, 18, and 27 layers of O, respectively. Figure 5(e) is a Sn-terminated surface and Fig. 4(l) is an O-terminated one. Although the top Sn and O atoms are not on the same plane as shown in Fig. 5(f), they are quite closer and can be treated as in the same surface layer. It also can be seen that although both of Fig. 5(f) and 4(k) are O- and Sn-terminated surfaces, their patterns of atom arrangements are quite different. On the surface, as shown in Fig. 5(f) Sn has five O coordinations while in Fig. 4(k) it only has four O coordinations. Actually, the
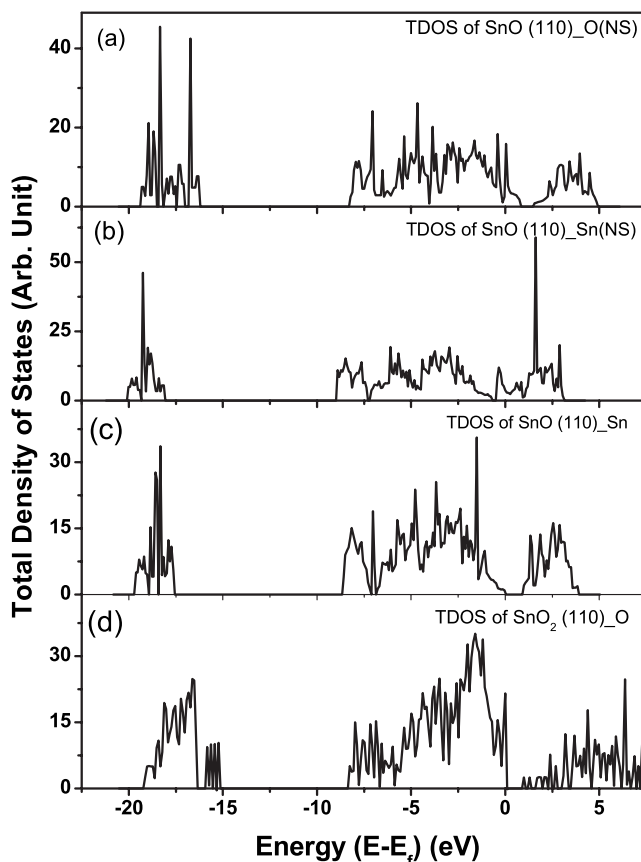
surfaces as shown in Figs. 4(k) and 4(l) are stoichiometric surfaces and Figs. 5(e) and 5(f) are the nonstoichiometric ones. Similar to the SnO (111) surface, unlike other low-index surfaces, the (111) surface is not an orthogonal rectangle repeat unit, instead, the angle between a and b axes is around 110°. Our calculated results also show that during formation of the (111) surfaces there exist obvious reconstructions, especially in Fig. 4(l) the top O atoms move toward the left side of the second layer Sn atoms. More details about the atom displacements are discussed in the next section.

Following Eq. (7), the calculated surface energies of the (111) stoichiometric surfaces of SnO and SnO_2 are 0.527, 2.072, and 1.887 J/m^2 for the surfaces shown in Figs. 4(j)–4(l), respectively. Obviously, the O-terminated (111) surface of SnO_2 [Fig. 4(l)] is more stable than the surface terminated both with O and Sn [Fig. 4(k)], and the surface energy of the (111) surface of SnO is lower than the corresponding (111) surfaces of SnO_2. If we only consider the stoichiometric surfaces of SnO_2, it can be seen from Table III that the SnO_2 (111) surface has the highest surface energy and is most unstable. This may be the part of the reason why this surface did not attract researchers' interests.

Following Eqs. (10a), (10b), (11a), (11b), (12a), and (12b), the surface free energies $[\gamma(p,T)]$ of the (111) sur-
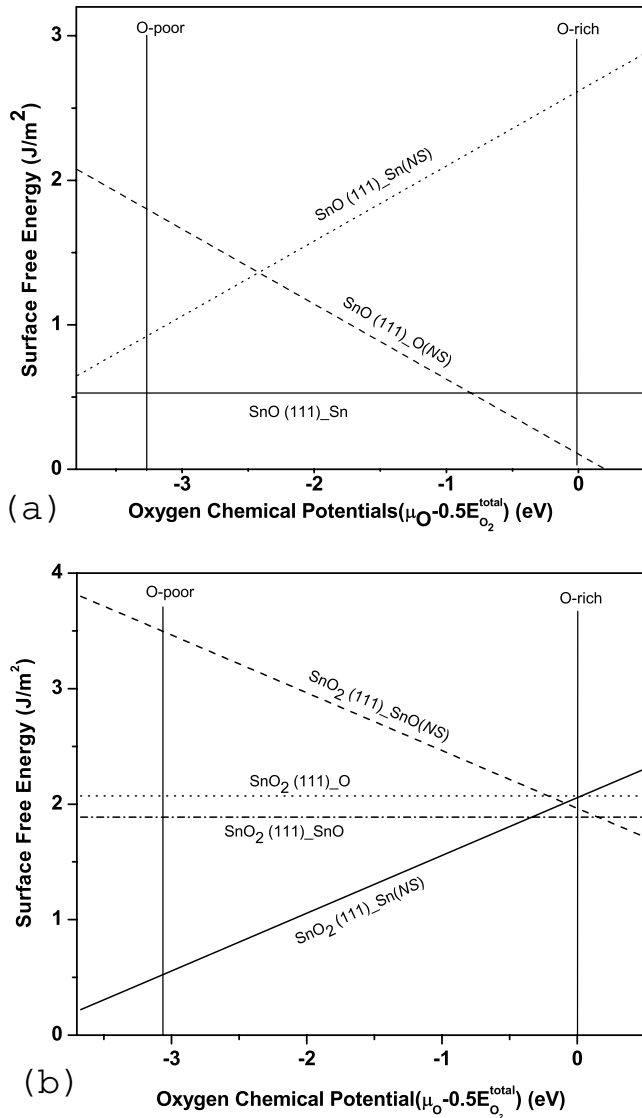
FIG. 12. The surface free energies of the (111) surfaces of SnO and SnO$_2$ versus the oxygen chemical potentials.

faces of SnO and SnO$_2$ are calculated with the different oxygen chemical potential [$\mu_O(p,T)$]. Figure 12 shows the relationship between $\gamma(p,T)$ and $\mu_O(p,T)$ for the (111) surfaces of SnO and SnO$_2$. Again in our scheme, the $\gamma(p,T)$ of the stoichiometric surfaces are constant within the whole rang of $\mu_O(p,T)$.

From Fig. 12(a), one can see that the $\gamma(p,T)$ of the Sn-terminated nonstoichiometric (111) surface of SnO [Fig. 5(d)] increases with increasing $\mu_O(p,T)$, and during the whole range of $\mu_O(p,T)$ it is greater than the $\gamma(p,T)$ of the corresponding stoichiometric surface, which means this kind of nonstoichiometric surface [Fig. 5(d)] is unstable. However, for the O-terminated nonstoichiometric surface as shown in Fig. 5(c), its $\gamma(p,T)$ decreases when $\mu_O(p,T)$ changes from O poor to O rich and when $\mu_O(p,T)$ close to reach O-rich bound the $\gamma(p,T)$ of this surface is lower than the corresponding stoichiometric ones, which means under O-rich condition with higher $\mu_O(p,T)$ this surface could be-

come more stable than the corresponding stoichiometric surface.

From Fig. 12(b), one can see that the $\gamma(p,T)$ of the Sn-terminated nonstoichiometric (111) surface of SnO$_2$ [Fig. 5(e)] increases with increasing $\mu_O(p,T)$, and interestingly, it is lower than the corresponding stoichiometric surfaces until $\mu_O(p,T)$ reach O-rich bound. This indicates that this nonstoichiometric symmetrical (111) surface of SnO$_2$ with Sn terminated could be stable when the $\mu_O(p,T)$ is not too high [<-0.5 eV in Fig. 12(b)] to reach its O-rich bound. For the O- and Sn-terminated nonstoichiometric surfaces shown in Fig. 5(f), its $\gamma(p,T)$ decreases when the $\mu_O(p,T)$ change from O poor to O rich and when $\mu_O(p,T)$ close to reach O-rich bound the $\gamma(p,T)$ of this surface is lower than the corresponding stoichiometric surface with O terminated, which means under O-rich condition with higher $\mu_O(p,T)$ this surface could become more stable than the corresponding stoichiometric surfaces.

The TDOS of the (111) surfaces of SnO and SnO$_2$ are shown in Figs. 13(a) and 13(b). From Fig. 13(a) one can see that for the nonstoichiometric surfaces of SnO there is no gap above Fermi level and the distance between two Sn layers is quite small [the second and third layers in Fig. 5(c), the first and second layers in Fig. 5(d)], all of these three layers are strongly binding and contribute to the surface states. For the O-terminated surface, the p orbitals of top O and the underneath Sn mainly form the surface states. However, in the Sn-terminated surface, the surface states are mainly from the top two layers of Sn. Compared to the stoichiometric (111) surface shown in the bottom of Fig. 13(a), the bands of Sn-terminated nonstoichiometric (111) surface are shifted to the lower energy part.

From Fig. 13(b), it can be seen that the TDOS for these four (111) SnO$_2$ surfaces are quite different. In the case of Sn-terminated surface shown in Fig. 5(e), the distance between the second layer of O and the third layer of Sn and O is quite small, therefore, both of them are interacting with the top layer of Sn to form surface states. Whereas in the case of the O-terminated surface as shown in Fig. 4(l) and in the lowest part of Fig. 13(b), the second layer of Sn atoms and part of the third layer O atoms are exposed to the surface, they are strongly contributing to the surface states. For the surfaces terminated both by Sn and O in Figs. 5(f) and 4(k), each Sn atom on the surface coordinates with five [Fig. 5(f)] or four [Fig. 4(k)] O atoms and each O atom coordinates with two Sn atoms. From their TDOS as shown in Fig. 13(b), it can be seen that there is a separate peak just below the Fermi level for the case of Sn coordinated with four O [Fig. 4(k)] which are mainly from the contributions of the top layer and the second layer of O.

7. Weak interactions in the low-index surfaces of SnO

From Figs. 4 and 5 it can be seen that all the low-index surfaces of SnO contain van der Waals (vdW) interactions. As demonstrated in Sec. II, including vdW interactions into DFT-GGA approach can precisely predict the structural and energetic properties of SnO. Carefully taking the boundary conditions of each surface as shown in Figs. 4 and 5, the
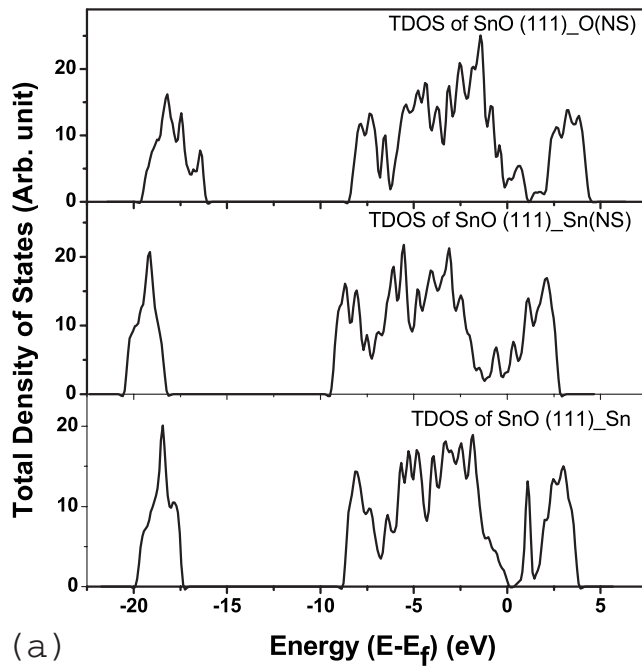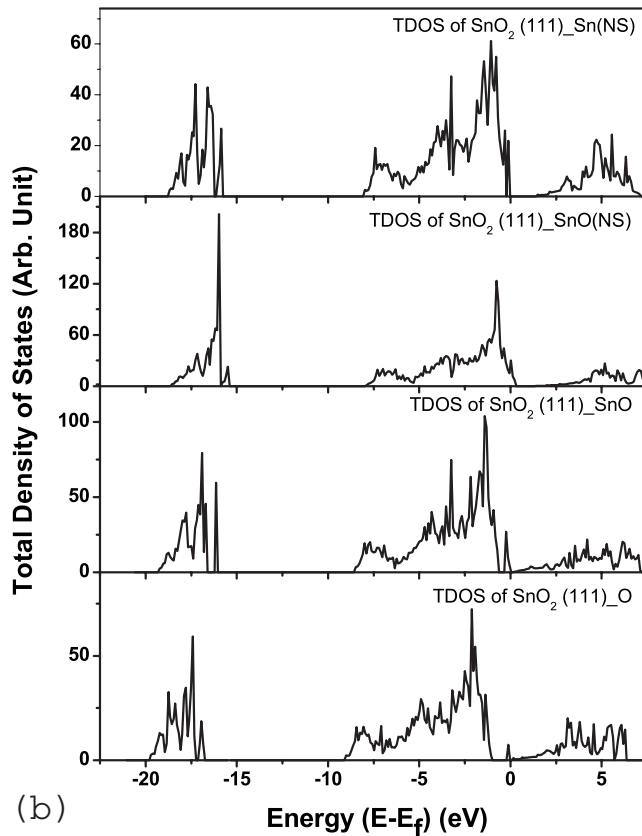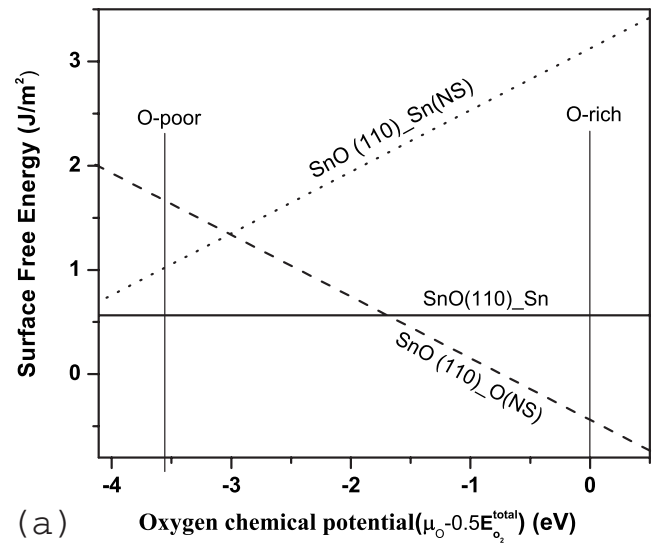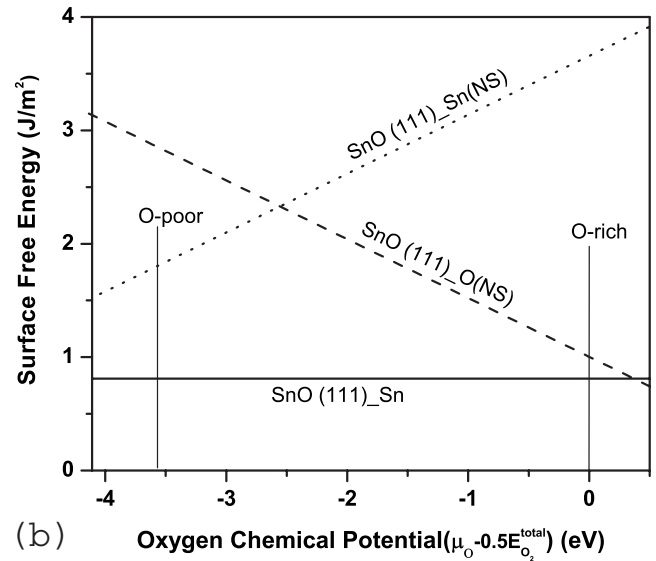
FIG. 13. The total density of states of the (111) surfaces of SnO (a) and SnO$_2$ (b).

FIG. 14. The surface free energies of the (110) and (111) surfaces of SnO versus the oxygen chemical potentials with the correction of van der Waals interactions.

vdW energy of each low-index surface can be calculated readily by following Eqs. (1)–(4). For the stoichiometric surfaces of SnO, the surface energy also can be calculated by Eq. (7), where the E_{slab} and E_{bulk} are obtained now by GGA+vdW for both the SnO bulk and its low-index surfaces. For non stoichiometric surfaces, following Eqs. (10b),

(11b), and (12b) the corresponding surface free energy $\gamma(p,T)$ can be calculated by including the vdW interactions into both the bulk and the surfaces.

The calculated surface energies (E_{surf}) of the stoichiometric surfaces of SnO are also listed in Table III. The calculated changes of $[\gamma(p,T)]$ for the nonstoichiometric surfaces [(110) and (111)] of SnO versus the oxygen chemical potentials $[\mu_{\mathrm{O}}(p,T)]$ are plotted in Figs. 14(a) and 14(b).

For SnO, compared to the bulk material, its low-index surfaces have lower symmetry, and the atoms on the surface layers are relaxed. Obviously, the calculated vdW energy of the bulk is lower than those of the low-index surfaces. Table III shows that the calculated surface energy of each SnO surface using DFT+vdW is higher than those using the DFT-GGA only approach, which means that all of the low-index surfaces using DFT+vdW become less stable. However, in both cases, as demonstrated in Table III, the relative stabilities of the low-index surfaces remain the same. Among them,

the (111) surface has the highest surface energy while the (001) surface has the lowest one and is most stable.

Comparing Fig. 14(a) with Fig. 10, one can see that after applying the vdW correction the surface free energy of the stoichiometric SnO (110) surface [Fig. 14(a)] moves up about 0.1 eV while the free energy curve of the O-terminated nonstoichiometric surface moves down about 0.5 eV, which means that this O-terminated nonstoichiometric (110) surface could be more stable than the corresponding stoichiometric one, shown in Fig. 4(h), when the $\mu_O(p,T)$ is greater than −1.5 eV as shown in Fig. 14(a). However, in the case of excluding the vdW correction, this O-terminated nonstoichiometric surface can be more stable than the stoichiometric one (Fig. 10) only when the $\mu_O(p,T)$ is quite high and reaches the O-rich bound. In both cases, with and without vdW corrections, the nonstoichiometric (110) surface with Sn terminated is unstable within the whole range of the oxygen chemical potentials. By comparing Fig. 14(b) with Fig. 12(a), when the vdW correction is included, the free energy of the SnO (111) stoichiometric surface increases about 0.3 eV, and all of the nonstoichiometric surfaces are unstable within the whole range of $\mu_O(p,T)$ as shown in Fig. 14(b). It also can be seen that in the case of excluding the vdW correction as shown in Fig. 12(a), when the $[\mu_O(p,T)]$ higher region up to the O-rich bound, the calculated $\gamma(p,T)$ of the O-terminated nonstoichiometric (111) surface of SnO could be lower than that of the corresponding stoichiometric one.

8. Stabilities of the low-index surfaces

Table III summarizes our calculated surface energies of the symmetrical stoichiometric low-index surfaces of SnO and SnO_2 and compares with the available results made by other researchers. From this table, one can see that each low-index can form at least one symmetrical stoichiometric surface. The calculated values of E_{surf} of the SnO_2 low-index surfaces are close to other reported results,[2,14,73] and the stabilities of the SnO_2 low-index surfaces are in the order (110)>(010)/(100)>(101)/(011)>(001)>(111). Except for the (111) surface, this order is the same as the one calculated by Oviedo and Gillan.[14] For the SnO_2 (111) surface, Mulheran and Harding[12] showed its excess energy is the second highest one. Our results show that this kind of surface has highest surface energy compared to other kinds of low-index surfaces.

For the low-index surfaces of SnO, unfortunately, there are no other data available to compare with. From this work either with or without the correction of the vdW interactions, the most stable surface is the (001) surface with Sn terminated. The stabilities of SnO low-index surfaces are approximately in the order (001)>(101)/(011)≈(010)/(100)>(110)>(111). The E_{surf} of the surface (010) or (100) is close to that of the (101) or (011) surface. Comparing to the (101) or (011) surface, the (010) O-terminated surface is a little bit more stable and its Sn-terminated surface is a little bit more unstable. As discussed above, for the same low-index surface, different termination causes a surface energy change and results in changing the order of their stabilities. From our calculated results, usually, the O-terminated sur-

face has a lower E_{surf} than the corresponding Sn-terminated surface does. For the same kind of low-index surface, both the O- and Sn-terminated surfaces are less stable than those with only O- or Sn-terminated surface. From Table III, it can be seen that overall the surfaces of SnO_2 have higher E_{surf} than the corresponding surfaces of SnO, which indicates that on the surface the Sn cannot hold high oxidation state (+4) and present with a reduced form.

C. Atom displacements during surface relaxation

During the formation of the surfaces, comparing to the atom positions in the bulk, the atoms on the surface layers are relaxed to compensate the dangling bonds or van der Waals interactions on the surface. Since the surface slabs still have two dimensional (assuming on xy plane) periodic boundary conditions like in their bulk, the atom positions shift along this plane should be small which are also proved from our calculated results. In most cases, the significant shift is along the z direction which is here assumed perpendicular to the surface plane. Tables IV and V list the surface atom position shifts compared to their corresponding positions in the bulk of SnO and SnO_2, respectively.

From Table IV it can be seen that on each layer the same kind of atoms could move to opposite directions (see those values with±sign) with the same amount of displacements. However, in the stoichiometric (110) and (111) surfaces [Figs. 4(h) and 4(j)], for the same group of atoms (in bulk they are identical by symmetrical operation) they can be relaxed not only to different directions but also with the different amount of displacements [e.g., Sn in Fig. 4(h) and O in Fig. 4(j)] which lead to symmetry broken. Table IV shows that to form the SnO (001) surface there is no displacement along xy plane and the displacement along z direction is also very small. Because to form this surface only simply needs to break the van der Waals weak bonds between the slices, both of the top Sn and the underneath O and Sn layers move up toward vacuum with a displacement less than 0.1 Å. As described in previous sections, this surface is the most stable one with small displacements. To form the (010) or (100) low-index surface, the O in the top Sn-O layer has a significant displacement of 0.14 Å along y direction whereas the Sn atom moves down along $−z$ with 0.08 Å. The atoms in the second and the third layers also have small movements into the slab (such as the second layer of O and the third layer of Sn) or up to the surface (such as the second layer of Sn and the third layer of O). Table IV shows that the atom displacements are different during formation of the (101) or (011) surfaces with different terminations: atoms in the O-terminated surface [Fig. 4(e)] have less displacement along xy plane than that in the Sn-terminated surface [Fig. 4(f)] has, and their displacements along $−z$ direction are less than 0.1 Å. In the case of the (110) surfaces, the Sn in the second layer of the O-terminated surface [Fig. 5(a)] has ±0.2 Å displacement as shown in Table IV and the atoms in the Sn-terminated nonstoichiometric surface [Fig. 5(b)] have small displacements along y and z, but the Sn in the first layer has ±0.1 Å displacement along x. From Table IV one can see that the atom displacements in the stoichiometric

TABLE IV. The atom displacements of the top three surface layers during formation of SnO surfaces (unit: Å). (Since the surfaces are symmetric, here we only show the upper part of the slab. For the corresponding atom in the other part, the displacement is the same, but the sign is its counterpart due to the symmetry. For z value, the negative sign means to move up toward vacuum, positive sign means to move into the surface slab.)

Surface	Structure	First layer	Second layer	Third layer
(001)	Fig. 4(a)	Sn(0.0,0.0,−0.062)	O(0.0,0.0,−0.053)	Sn(0.0,0.0,−0.013)
(010)/(100)	Fig. 4(c)	O(0.0,−0.136,0.039)	O(0.0,−0.084,0.003)	O(0.0,−0.016,−0.023)
		Sn(0.0,−0.046,0.078)	Sn(0.0,−0.085,−0.099)	Sn(0.0,−0.027,0.026)
(101)/(011)	Fig. 4(e)	O(0.0,−0.034,0.096)	Sn(0.0,0.070,0.073)	O(0.0,−0.015,0.064)
	Fig. 4(f)	Sb(0.0,−0.114,0.064)	O(0.0,−0.011,0.01)	O(0.0,0.043,−0.062)
(110)	Fig. 4(h)	Sn(0.449,0.0,−0.435)	O(0.377, ± 0.044,−0.077)[a]	Sn(0.220,0.0,0.160)
				Sn(0.080,0.0,−0.095)
	Fig. 5(a)	O(0.0,0.0,0.056)	Sn(±0.231,0.0,−0.209)[a]	O(0.0,0.0,0.031)
	Fig. 5(b)	Sn(±0.103,0.0,−0.036)[a]	O(0.0,0.0,0.023)	Sn(±0.027,0.0,0.004)[a]
(111)	Fig. 4(j)	Sn(0.021,0.049,−0.396)	O(0.051,0.217,−0.193)	Sn(0.092,0.212,−0.037)
			O(0.137,0.217,−0.193)	
	Fig. 5(c)	O(0.439,1.034,−0.304)	Sn(0.110,0.253,0.074)	Sn(0.192,0.442,−0.889)
	Fig. 5(d)	Sn(0.282,0.652,0.249)	Sn(0.231,0.532,−0.621)	O(0.023,0.035,0.0)

[a]± means that half of the atoms of that layer move in opposite direction related to the other half.

SnO (110) surface [Fig. 4(j)] are larger than those in nonstoichiometric ones. Because this surface was obtained by cleaving half Sn of the top surface layer as shown in Fig. 5(b), to make up this extra cleavage, larger atom relaxations are expected. The behavior of the nonstoichiometric (111) surfaces of SnO formation [Figs. 5(c) and 5(d)] is quite different from its other low-index surfaces as shown in Table IV in which larger atom displacements on both xy plane and

along z direction are found. Overall, the atom displacement is decreased from top layer atom to the inner layer ones because the inner layers are close to the bulk behavior.

In order to explore the possibility of reconstruction on the pure surfaces of SnO, the supersurface cells for these stoichiometric low-index surfaces are expanded to (2×2). The same relaxation calculations have been performed on these 2×2 supercells as the same as we did for (1×1) supersur-

TABLE V. The atom displacements of the top three surface layers during formation of SnO_2 surfaces (Unit: Å). (Since we have symmetric surface, here we only show the upper part of the slab. For the corresponding atom in the other part, the displacement is the same, but the sign is its counterpart due to the symmetry. For z value, the negative sign means move up toward the vacuum, positive sign means move into the surface slab.)

Surface	Structure	First layer	Second layer	Third layer
(001)	Fig. 4(b)	O(0.088,0.088,−0.1367)	O(0.029,−0.029,0.063)	O(0.001,0.001,−0.049)
		Sn(0.0,0.0,0.193)	Sn(0.0,0.0,−0.145)	Sn(0.0,0.0,0.062)
(010)/(100)	Fig. 4(d)	O(0.267,0.0,−0.171)	Sn(−0.066,0.0,−0.039)	O(0.133,0.0,−0.113)
(101)/(011)	Fig. 4(g)	O(0.021,0.050,−0.053)	Sn(0.054,0.200,0.030)	O(0.011,−0.020,−0.091)
(110)	Fig. 4(i)	O(0.0,0.0,−0.049)	O(0.0,−0.056,−0.175)	O(0.0,0.0,−0.031)
			Sn(0.0,0.0,−0.180)	
(111)	Fig. 4(k)	O(−0.325,−0.100,−0.295)[a]	O(−0.299,−0.299,0.138)	Sn(0.122,0.122,−0.088)
		Sn(−0.392,−0.392,0.042)		
	Fig. 4(l)	O(−1.713,−1.713,−0.700)	Sn(0.074,0.074,0.027)	O(−0.026,−0.026,−0.087)
	Fig. 5(e)	Sn(0.070,0.070,−0.055)	O(−0.031,−0.031,−0.128)	O(−0.028,0.002,−0.107)[a]
				Sn(0.088,0.088,0.213)
	Fig. 5(f)	O(−0.054,−0.054,−0.083)	O(−0.321,−0.082,−0.148)[a]	O(0.062,0.062,−0.030)
			Sn(0.059,0.059,0.200)	

[a]In those layers there is another type of O atom which is displaced by O(y, x, z) where the x, y, and z values are those indicated in the table as (x', y', z') with $x' = y$, $y' = x$, and $z' = z$.

face cells. The calculated surface energies (E_{surf}) are 0.0816, 0.390, 0.408, 0.360, 0.484, and 0.539 J/m² for (001), (010)/(100), (101)/(011)_Sn, (101)/(011)_O, (110), and (111) surfaces of SnO respectively. Comparing these values with those listed in Table III for (1×1) supercells, the differences are very small: the (001), (010)/(100), and (101) with Sn-terminated surfaces have the differences less than 1.0%, the (110) surface has a largest error with 3.8%. By checking the atomic displacements in these large supercells, the directions of relaxations are very similar to those listed in Table IV. Moreover, there are some differences in the amount of displacements of each atom group compared to the numbers listed in Table IV, but these differences are relatively small. These results indicate that there are no obvious reconstructions on these nondefective pure low-index surfaces of SnO.

From Table V, it can be seen that the most stable (110) surface of SnO_2 has smaller atom displacements compared to its other surfaces. Interestingly, most of the atoms on the first layer move up toward the vacuum. To form the (001) surface, the O atoms in the top layer move up to the vacuum while the Sn atoms move into the slab. The atoms in the third layer have the similar behavior with small displacements while the atoms in the second layer have opposite displacements. Table V shows that the formation of the (101) or (011) surface of SnO_2 is quite similar to the formation of the (010) or (100) surface of SnO_2. The only difference between them is that instead of moving into slab, the second layer of Sn atoms in the (100) surface move up to the surface by less than 0.1 Å. Similar to its (001) surface, the atom displacements along xy plane in the (110) surface are quite small, and all atoms move up toward the vacuum which are similar to other reported results.[6,9,14,72] Similar to SnO, the formation of the SnO_2 (111) surfaces is quite different from their other surfaces. They have large atom displacements not only along the z direction but also along xy plane. The O atom in the O-terminated (111) surface as shown in Fig. 4(l) has a largest displacement of 1.7 Å along the xy plane and 0.7 Å along z direction, which indicate that this kind of surface has a significant reconstruction during formation. In this case the top O with unsaturated bonding shown in Fig. 4(l) tends to bond with the closest Sn in the second layer to form a reconstructed surface. Such kind of surface relaxation and reconstruction also was investigated and observed in (110) surface at high annealing temperatures by Batzill *et al.*[8] Compared to other (111) surfaces, the (111) surface with Sn terminated as shown in Fig. 5(e) has smaller atom displacements, which means this surface could be stable. The calculated relationship between $\gamma(p,T)$ and $\mu_O(p,T)$ for the (111) surfaces of SnO_2 as shown in Fig. 12(b) does show that this surface could be stable when $\mu_O(p,T)$ close to the O-poor region.

IV. SUMMARY AND CONCLUSIONS

The structural and electronic properties of the bulk and low-index surfaces of SnO and SnO_2 have been investigated by density functional approach within the GGA with PAW pseudopotentials. An empirical method has been adopted in this study to account for the vdW interactions among the

Sn-O layers in the bulk and low-index surfaces of SnO. Our results show that compared with SnO_2, the structural and electronic properties for SnO bulk and low-index surfaces present some unique features.

Due to the dual valency of Sn, the bulk behaviors of the SnO and SnO_2 are quite different. The calculated band gap of SnO_2 is direct with value of 0.69 eV while in SnO is an indirect one with value of 0.32 eV. In both cases, due to the DFT approximation, the calculated values are much lower than the experimental measurements although our calculated band gaps are in good agreement with other theoretical reported results. In both SnO and SnO_2, the second valence band with lower energy is dominated by O s orbital. The first valence band and the conduction band are formed by the O p orbitals with s, p, and d orbitals of Sn. The electronic density of states reveals that for SnO, below the Fermi level in the first valence band the s orbital of Sn has a larger contribution than its p and d orbitals have, and above the Fermi level in the conduction band the p orbitals of Sn have larger contribution than its s and d orbitals have. The d orbital of Sn does not contribute much in the valence band and the lower part of its conduction band. However in the SnO_2 bulk, in the upper part of the first valence band the p and d orbitals of Sn play an important role and its s orbital dominates to form the lower part of the first valence band. In the lower part of the conduction band, the s orbital of Sn has a bigger contribution than its p and d orbitals have. The upper part of the conduction band is mainly dominated by p and d orbitals of Sn. In both SnO and SnO_2, the s orbital of O has lower energy and contributes to the second valence band with lower energy. The p orbital of O is involved in bonding in the first valence band and the conduction band. By calculating the total binding energy versus the volume change and fitted to the Birch-Murnaghan equation of state, the calculated bulk modulus and cohesive energy are close to the experimental measurements and other calculated results.

By constructing all possible low-index symmetric surfaces of SnO and the (111) surface of SnO_2, our results reveal that the surface energies of the SnO low-index surfaces are lower than the corresponding surfaces of SnO_2 due to different bonding between Sn and O in these two oxides, and in the SnO low-index surfaces there are van der Waals weak interactions to binding SnO slices together whereas in the case of SnO_2 the interactions are strong chemical bonding. For the same kind of low-index, the O-terminated surface usually is more stable than the corresponding Sn-terminated surface, and both of them are more stable than the same index surfaces with both O and Sn terminated. Among low-index surfaces of SnO, the (001) surface has a lowest surface energy, whereas in the case of SnO_2, the (110) surface is the most stable one. With both the DFT-GGA and GGA+vdW approaches, the calculated stabilities of the low-index stoichiometric symmetrical surfaces of SnO are in the same order $(001) > (101)/(011) \gtrsim (010)/(100) > (110) > (111)$. Moreover, the calculated order of stabilities of SnO_2 surfaces is $(110) > (010)/(100) > (101)/(011) > (001) > (111)$, which are in good agreement with other reported results. There is no theoretical study for the SnO_2 (111) surface in the literature. Our results show that the (111) surfaces of SnO_2 with different terminations have highest surface energies and are least stable.

By calculating the surface free energy $[\gamma(p,T)]$ with the oxygen chemical potential $[\mu_O(p,T)]$, we can explore the stabilities of the surfaces under different conditions, such as $\mu_O(p,T)$, pressure, temperature, etc. Our results indicate that the $\gamma(p,T)$ can be changed by varying $\mu_O(p,T)$ and under some conditions the unstable surface (especially for the non-stoichiometric) can become more stable than the corresponding stoichiometric ones (as shown in Figs. 10 and 12). The O-terminated nonstoichiometric (110) and (111) surfaces of SnO and the (111) surface of SnO$_2$ could be more stable than their corresponding stoichiometric ones under O-rich condition with higher $\mu_O(p,T)$. When considering vdW interactions, the O-terminated nonstoichiometric (110) surface of SnO could become more stable than its corresponding stoichiometric one under moderate conditions of $\mu_O(p,T)$ as shown in Fig. 14(a). Interestingly, the Sn-terminated (111) nonstoichiometric surface of SnO$_2$ could be stable when $\mu_O(p,T)$ is low in the O-poor region. Our results show that the Sn-terminated (110) and (111) nonstoichiometric surfaces of SnO are always unstable when $\mu_O(p,T)$ is increased from O-poor to O-rich bound.

By combining vdW interactions with DFT-GGA, as shown in Table II, the calculated structure parameters and bulk modulus of bulk SnO are closer to the experimental measurements. The calculated surface energies of the low-index surfaces of SnO are larger than those without applying the vdW correction as listed in Table III. These results show that the DFT-GGA scheme does not fully handle the interactions between the SnO layers among the bulk and low-index surfaces of SnO because these interactions are dominated by van der Waals forces which are not described well in the current DFT-GGA scheme. Therefore, the vdW correction is needed to deal with SnO and its low-index surfaces. Interestingly, although in both cases (with or without vdW correction), the values of the calculated surface energy for each surface are different as demonstrated in Table III, the relative stabilities of these low-index surfaces remain the same. Since there are no experimental or other theoretical values available to compare with, our results shown in Table III could be the best estimations of the real surface energies of the SnO low-index surfaces.

Our results indicate that the differences between SnO$_2$ and SnO are significant and the convertible transition of Sn$^{4+} \leftrightarrow$ Sn^{2+} may have a great application. Our calculation results show that the SnO$_2$ is the most stable form of the tin oxides and the SnO is favorable to convert to SnO$_2$ when O$_2$ is presented. The SnO$_2$ could be decomposed to SnO and O$_2$ only at very high temperature and very low O$_2$ pressure. Compared to SnO$_2$, the electronic properties of the SnO low-index surfaces have some unique features and the van der Waals interactions in the surfaces of SnO may lead to more active sites for interacting with other molecules. These special features of tin oxides could be used to develop high-temperature sensor-related applications.

*Author to whom correspondence should be addressed; FAX: 412-386-4542; duany@netl.doe.gov

[1] M. Batzill, Sensors-Basel **6**, 1345 (2006).

[2] M. Batzill and U. Diebold, Prog. Surf. Sci. **79**, 47 (2005).

[3] Z. Chen and C. Lu, Sens. Lett. **3**, 274 (2005).

[4] E. Comini, Anal. Chim. Acta **568**, 28 (2006).

[5] K. Katsiev, M. Batzill, U. Diebold, A. Urban, and B. Meyer, Phys. Rev. Lett. **98**, 186102 (2007).

[6] A. Atrei, E. Zanazzi, U. Bardi, and G. Rovida, Surf. Sci. **475**, L223 (2001).

[7] M. Batzill, K. Katsiev, and U. Diebold, Surf. Sci. **529**, 295 (2003).

[8] M. Batzill, K. Katsiev, J. M. Burst, U. Diebold, A. M. Chaka, and B. Delley, Phys. Rev. B **72**, 165414 (2005).

[9] W. Bergermayer and I. Tanaka, Appl. Phys. Lett. **84**, 909 (2004).

[10] V. Caslavska and R. Roy, J. Appl. Phys. **40**, 3414 (1969).

[11] S. Choudhury, C. A. Betty, K. G. Girija, and S. K. Kulshreshtha, Appl. Phys. Lett. **89**, 071914 (2006).

[12] P. A. Mulheran and J. H. Harding, Modell. Simul. Mater. Sci. Eng. **1**, 39 (1992).

[13] J. Oviedo and M. J. Gillan, Surf. Sci. **467**, 35 (2000).

[14] J. Oviedo and M. J. Gillan, Surf. Sci. **463**, 93 (2000).

[15] J. Oviedo and M. J. Gillan, Surf. Sci. **490**, 221 (2001).

[16] J. Oviedo and M. J. Gillan, Surf. Sci. **513**, 26 (2002).

[17] L. S. Roman, R. Valaski, C. D. Canestraro, E. C. S. Magalhaes, C. Persson, R. Ahuja, E. F. da Silva, I. Pepe, and A. F. da Silva, Appl. Surf. Sci. **252**, 5361 (2006).

[18] Y. Yamaguchi, K. Tabata, and E. Suzuki, Surf. Sci. **526**, 149 (2003).

[19] L. Gracia, A. Beltran, and J. Andres, J. Phys. Chem. B **111**, 6479 (2007).

[20] R. A. Evarestov, A. V. Bandura, and E. V. Proskurov, Phys. Status Solidi B **243**, 1823 (2006).

[21] A. V. Bandura, J. O. Sofo, and J. D. Kubicki, J. Phys. Chem. B **110**, 8386 (2006).

[22] K. Suito, N. Kawai, and Y. Masuda, Mater. Res. Bull. **10**, 677 (1970).

[23] F. Lawson, Nature (London) **215**, 955 (1967).

[24] D. R. Lide, *CRC Handbook of Chemistry and Physics* (CRC, Boca Raton, FL, 2002).

[25] V. M. Jimenez, J. A. Mejias, J. P. Espinos, and A. R. Gonzalez-Elipe, Surf. Sci. **366**, 545 (1996).

[26] C. L. Lau and G. K. Wertheim, J. Vac. Sci. Technol. **15**, 622 (1978).

[27] J. M. Themlin, M. Chtaib, L. Henrard, P. Lambin, J. Darville, and J. M. Gilles, Phys. Rev. B **46**, 2460 (1992).

[28] V. M. Jimenez, G. Lassaletta, A. Fernandez, J. P. Espinos, F. Yubero, A. R. Gonzalez-Elipe, L. Soriano, J. M. Sanz, and D. A. Papaconstantopoulos, Phys. Rev. B **60**, 11171 (1999).

[29] M. Meyer, G. Onida, M. Palummo, and L. Reining, Phys. Rev. B **64**, 045119 (2001).

[30] G. W. Watson, J. Chem. Phys. **114**, 758 (2001).

[31] A. Walsh and G. W. Watson, Phys. Rev. B **70**, 235114 (2004).

[32] L. A. Errico, Physica B **389**, 140 (2007).

[33] G. Kresse and J. Hafner, Phys. Rev. B **47**, 558 (1993).

[34] G. Kresse and J. Furthmuller, Phys. Rev. B **54**, 11169 (1996).

[35] G. Kresse and J. Furthmuller, Comput. Mater. Sci. **6**, 15 (1996).

[36] P. E. Blochl, Phys. Rev. B **50**, 17953 (1994).

[37] G. Kresse and D. Joubert, Phys. Rev. B **59**, 1758 (1999).

[38] D. Vanderbilt, Phys. Rev. B **41**, 7892 (1990).

[39] J. P. Perdew, J. A. Chevary, S. H. Vosko, K. A. Jackson, M. R. Pederson, D. J. Singh, and C. Fiolhais, Phys. Rev. B **46**, 6671 (1992).

[40] J. P. Perdew, K. Burke, and M. Ernzerhof, Phys. Rev. Lett. **77**, 3865 (1996).

[41] H. J. Monkhorst and J. D. Pack, Phys. Rev. B **13**, 5188 (1976).

[42] Q. Wu and W. Yang, J. Chem. Phys. **116**, 515 (2002).

[43] D. C. Langreth, M. Dion, H. Rydberg, E. Schroder, P. Hyldgaard, and B. I. Lundqvist, Int. J. Quantum Chem. **101**, 599 (2005).

[44] W. J. Moore and L. Pauling, J. Am. Chem. Soc. **63**, 1392 (1941).

[45] J. Pannetier and G. Denes, Acta Crystallogr., Sect. B: Struct. Crystallogr. Cryst. Chem. **36**, 2763 (1980).

[46] M. Dion, H. Rydberg, E. Schroder, D. C. Langreth, and B. I. Lundqvist, Phys. Rev. Lett. **92**, 246401 (2004).

[47] U. Zimmerli, M. Parrinello, and P. Koumoutsakos, J. Chem. Phys. **120**, 2693 (2004).

[48] S. Grimme, J. Antony, T. Schwabe, and C. Muck-Lichtenfeld, Org. Biomol. Chem. **5**, 741 (2007).

[49] M. Elsner, P. Hobza, T. Frauenheim, S. Suhai, and E. Kaxiras, J. Chem. Phys. **114**, 5149 (2001).

[50] S. Grimme, J. Comput. Chem. **25**, 1463 (2004).

[51] M. Hasegawa and K. Nishidate, Phys. Rev. B **70**, 205431 (2004).

[52] K. Ellmer, J. Phys. D **34**, 3097 (2001).

[53] G. J. McCarthy and J. M. Welton, Powder Diffr. **4**, 156 (1989).

[54] F. Birch, Phys. Rev. **71**, 809 (1947).

[55] F. D. Murnaghan, Am. J. Math. **59**, 235 (1937).

[56] A. C. Camargo, J. A. Igualada, A. Beltran, R. Llusar, E. Longo, and J. Andres, Chem. Phys. **212**, 381 (1996).

[57] J. Haines and J. M. Leger, Phys. Rev. B **55**, 11144 (1997).

[58] M. A. Maki-Jaskari and T. T. Rantala, Phys. Rev. B **64**, 075407 (2001).

[59] K. C. Mishra, K. H. Johnson, and P. C. Schmidt, Phys. Rev. B **51**, 13972 (1995).

[60] O. N. Mryasov and A. J. Freeman, Phys. Rev. B **64**, 233111 (2001).

[61] J. Geurts, S. Rau, W. Richter, and F. J. Schmitte, Thin Solid Films **121**, 217 (1984).

[62] K. M. Krishna, M. Sharon, M. K. Mishra, and V. R. Marathe, Electrochim. Acta **41**, 1999 (1996).

[63] N. E. Christensen, A. Svane, and E. L. Pettzery Blanca, Phys. Rev. B **72**, 014109 (2005).

[64] Y. Yamaguchi, K. Tabata, and T. Yashima, J. Mol. Struct.: THEOCHEM **714**, 221 (2005).

[65] C. Ambrosch-Draxl and J. O. Sofo, Comput. Phys. Commun. **175**, 1 (2006).

[66] J. J. Xie, S. de Gironcoli, S. Baroni, and M. Scheffler, Phys. Rev. B **59**, 970 (1999).

[67] S. Cristol, J. F. Paul, E. Payen, D. Bougeard, S. Clemendot, and F. Hutschka, J. Phys. Chem. B **104**, 11220 (2000).

[68] M. Batzill and U. Diebold, J. Phys.: Condens. Matter **18**, L129 (2006).

[69] M. Batzill, K. Katsiev, J. M. Burst, Y. Losovyj, W. Bergermayer, I. Tanaka, and U. Diebold, J. Phys. Chem. Solids **67**, 1923 (2006).

[70] S. P. Bates, G. Kresse, and M. J. Gillan, Surf. Sci. **385**, 386 (1997).

[71] K. Reuter and M. Scheffler, Phys. Rev. B **65**, 035406 (2007).

[72] T. T. Rantala, T. S. Rantala, and V. Lantto, Surf. Sci. **420**, 103 (1999).

[73] A. Beltran, J. Andres, E. Longo, and E. R. Leite, Appl. Phys. Lett. **83**, 635 (2003).